



Impacts of an unknown daytime HONO source on the mixing ratio and budget of HONO, and hydroxyl, hydroperoxyl, and organic peroxy radicals, in the coastal regions of China

Y. Tang^{1,2}, J. An¹, F. Wang^{1,2,3}, Y. Li¹, Y. Qu¹, Y. Chen¹, and J. Lin^{1,2}

¹State Key Laboratory of Atmospheric Boundary Layer Physics and Atmospheric Chemistry (LAPC), Institute of Atmospheric Physics (IAP), Chinese Academy of Sciences, Beijing 100029, China

²University of the Chinese Academy of Sciences, Beijing 100049, China

³Anhui Meteorological Bureau, Hefei 230061, China

Correspondence to: J. An (anj@mail.iap.ac.cn)

Received: 16 November 2014 – Published in Atmos. Chem. Phys. Discuss.: 9 January 2015

Revised: 3 July 2015 – Accepted: 2 August 2015 – Published: 21 August 2015

Abstract. Many field experiments have found high nitrous acid (HONO) mixing ratios in both urban and rural areas during daytime, but these high daytime HONO mixing ratios cannot be explained well by gas-phase production, HONO emissions, and nighttime hydrolysis conversion of nitrogen dioxide (NO₂) on aerosols, suggesting that an unknown daytime HONO source (P_{unknown}) could exist. The formula $P_{\text{unknown}} \approx 19.60[\text{NO}_2] \cdot J(\text{NO}_2)$ was obtained using observed data from 13 field experiments across the globe. The three additional HONO sources (i.e., the P_{unknown} , nighttime hydrolysis conversion of NO₂ on aerosols, and HONO emissions) were coupled into the WRF-Chem model (Weather Research and Forecasting model coupled with Chemistry) to assess the P_{unknown} impacts on the concentrations and budgets of HONO and peroxy (hydroxyl, hydroperoxyl, and organic peroxy) radicals (RO_x) (= OH + HO₂ + RO₂) in the coastal regions of China. Results indicated that the additional HONO sources produced a significant improvement in HONO and OH simulations, particularly in the daytime. High daytime average P_{unknown} values were found in the coastal regions of China, with a maximum of 2.5 ppb h⁻¹ in the Beijing–Tianjin–Hebei region. The P_{unknown} produced a 60–250 % increase of OH, HO₂, and RO₂ near the ground in the major cities of the coastal regions of China, and a 5–48 % increase of OH, HO₂, and RO₂ in the daytime meridional-mean mixing ratios within 1000 m above the ground. When the three additional HONO sources were included, the photolysis of HONO was the second most important source in

the OH production rate in Beijing, Shanghai, and Guangzhou before 10:00 LST with a maximum of 3.72 ppb h⁻¹ and a corresponding P_{unknown} contribution of 3.06 ppb h⁻¹ in Beijing, whereas the reaction of HO₂ + NO (nitric oxide) was dominant after 10:00 LST with a maximum of 9.38 ppb h⁻¹ and a corresponding P_{unknown} contribution of 7.23 ppb h⁻¹ in Beijing. The whole RO_x cycle was accelerated by the three additional HONO sources, especially the P_{unknown} . The daytime average OH production rate was enhanced by 0.67 due to the three additional HONO sources; [0.64], due to the P_{unknown} , to 4.32 [3.86] ppb h⁻¹, via the reaction of HO₂ + NO, and by 0.49 [0.47] to 1.86 [1.86] ppb h⁻¹, via the photolysis of HONO. The OH daytime average loss rate was enhanced by 0.58 [0.55] to 2.03 [1.92] ppb h⁻¹, via the reaction of OH + NO₂, and by 0.31 [0.28] to 1.78 [1.64] ppb h⁻¹, via the reaction of OH + CO (carbon monoxide) in Beijing, Shanghai, and Guangzhou. Similarly, the three additional HONO sources produced an increase of 0.31 [0.28] (with a corresponding P_{unknown} contribution) to 1.78 [1.64] ppb h⁻¹, via the reaction of OH + CO, and 0.10 [0.09] to 0.63 [0.59] ppb h⁻¹, via the reaction of CH₃O₂ (methylperoxy radical) + NO in the daytime average HO₂ production rate, and 0.67 [0.61] to 4.32 [4.27] ppb h⁻¹, via the reaction of HO₂ + NO in the daytime average HO₂ loss rate in Beijing, Shanghai, and Guangzhou. The above results suggest that the P_{unknown} considerably enhanced the RO_x concentrations and accelerated RO_x cycles in the coastal regions of China, and could produce significant increases in concentrations of in-

organic aerosols and secondary organic aerosols and further aggravate haze events in these regions.

1 Introduction

The hydroxyl radical (OH) is the most dominant oxidant in the troposphere, initiating daytime photochemistry, removing the majority of reactive gases, and leading to the formation of secondary products (e.g., ozone (O₃), PANs (peroxyacyl nitrates), and aerosol) that can affect air quality, climate, and human health (Stone et al., 2012). OH is formed primarily through the photolysis of O₃, nitrous acid (HONO), hydrogen peroxide (H₂O₂), the reactions of O₃ with alkenes, and the hydroperoxyl radical (HO₂) to OH conversion process (HO₂+NO) (Platt et al., 1980; Crutzen and Zimmermann, 1991; Atkinson and Aschmann, 1993; Fried et al., 1997; Paulson et al., 1997). Recent field experiments have found that the contribution of the photolysis of HONO to daytime OH production can reach up to 56, 42, and 33% in urban, rural and forest areas, respectively (Ren et al., 2003; Kleffmann et al., 2005; Acker et al., 2006), more than that of the photolysis of O₃. However, most current air quality models fail to predict observed HONO concentrations, underestimating daytime HONO in particular (Czader et al., 2012; Gonçalves et al., 2012; Li et al., 2011), due to the incomplete knowledge of HONO sources.

It is generally accepted that the photolysis of HONO (Reaction R2) in the early morning could be a major source of OH. After sunrise, HONO mixing ratios are usually in low concentrations due to the strong photolysis of HONO. However, many field experiments have found daytime HONO mixing ratios that are unexpectedly higher than the theoretical steady value (~10 ppt), in both urban and rural areas: e.g., 0.15–1.50 ppb in Asia (Su et al., 2008; Wu et al., 2013; Spataro et al., 2013), 0.01–0.43 ppb in Europe (Kleffmann et al., 2005; Acker and Möller, 2007; Sörgel et al., 2011; Michoud et al., 2014), 0.02–0.81 ppb in North America (Zhou et al., 2002a, b; Ren et al., 2010; Villena et al., 2011; N. Zhang et al., 2012; Wong et al., 2012; VandenBoer et al., 2013), 2.00 ppb (maximum) in South America (Elshorbany et al., 2009), and 0.015–0.02 ppb in Antarctica (Kerbrat et al., 2012) (Fig. 1). These high HONO mixing ratios, particularly in the daytime, cannot be explained well by gas-phase production (Reaction R1), HONO emissions, and nighttime hydrolysis conversion of NO₂ on aerosols, suggesting that an unknown daytime HONO source (*P*_{unknown}) could exist.



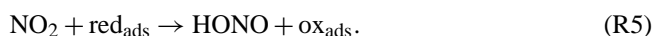
The *P*_{unknown} was calculated by Su et al. (2008) at Xinken (Guangzhou, China), with a maximum of 4.90 ppb h⁻¹. Spataro et al. (2013) proposed a *P*_{unknown} value of

2.58 ppb h⁻¹ in Beijing. In fact, *P*_{unknown} values, ranging from 0.06 to 4.90 ppb h⁻¹, have been obtained from many field studies across the globe, as shown in Fig. 1, suggesting *P*_{unknown} could contribute greatly to the daytime production of OH and HO₂.

The most important formation pathway for nocturnal HONO could be the hydrolysis reaction of nitrogen dioxide (NO₂) on humid surfaces (Reaction R4) (Kleffmann et al., 1999; Alicke et al., 2002; Finlayson-Pitts et al., 2003):



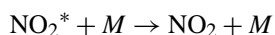
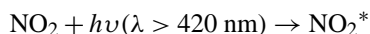
Ammann et al. (1998) found HONO formation via the heterogeneous reduction of NO₂ on the surface of soot (Reaction R5), and Reaction (R5) can be enhanced by irradiation (Monge et al., 2010):



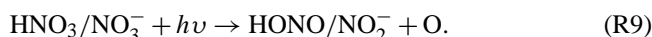
George et al. (2005) and Stemmler et al. (2006, 2007) showed the heterogeneous reduction of NO₂ on organic surfaces (Reaction R6) (e.g., humic acid) to produce HONO:



Li et al. (2008) proposed a homogeneous reaction of photolytically excited NO₂ with H₂O (Reaction R7), but this reaction has been proven to be unimportant in the real atmosphere (Carr et al., 2009; Wong et al., 2011; Amedro et al., 2011). Zhang and Tao (2010) suggested the homogeneous nucleation of NO₂, H₂O, and ammonia (NH₃) for the production of HONO (Reaction R8), but Reaction (R8) has not yet been tested in laboratory studies, nor observed in field experiments:



Zhou et al. (2002b, 2003, 2011) demonstrated that the photolysis of adsorbed nitric acid (HNO₃) and nitrate (NO₃⁻) at ultraviolet wavelengths (~300 nm) (Reaction R9) can produce HONO:



Additionally, HONO could be emitted from soils (Su et al., 2011; Oswald et al., 2013), and may be important in farmland and forest areas.

Based on these mechanisms outlined above, some modeling studies have been carried out to simulate HONO concentrations (e.g., An et al., 2011; Czader et al., 2012; Gonçalves et al., 2012). Sarwar et al. (2008) incorporated Reactions (R4), (R9), and HONO emissions into the Community Multiscale Air Quality (CMAQ) model, but still underestimated HONO mixing ratios during daytime. Li et

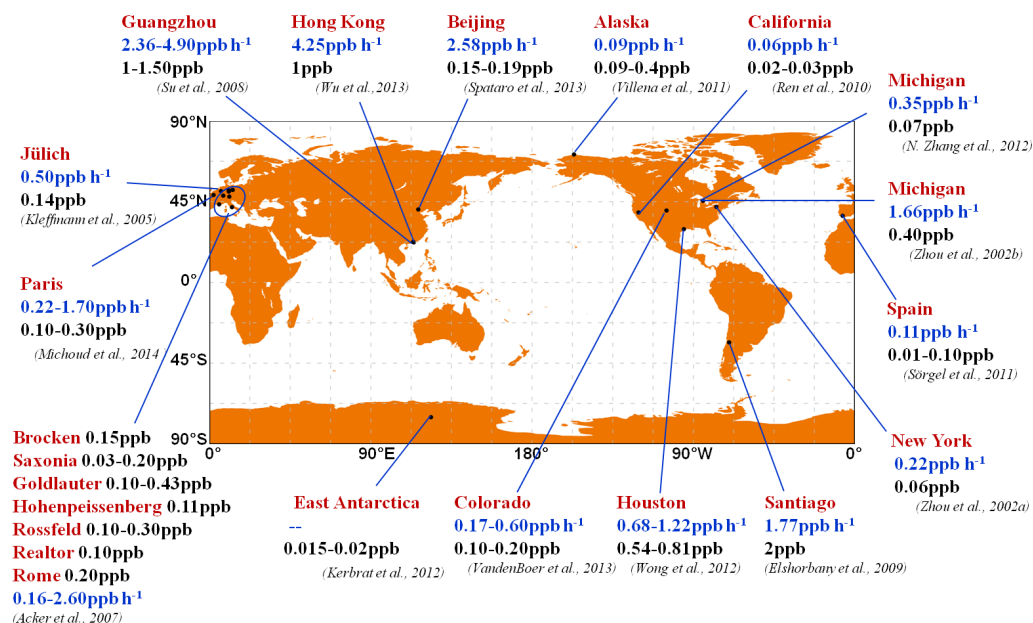


Figure 1. Summary of observed HONO mixing ratios at noon (black font) and the calculated unknown daytime HONO source (blue font) from field studies.

al. (2010) considered both aerosol and ground surface reactions, and HONO emissions, in the WRF-Chem model (Weather Research and Forecasting model coupled with Chemistry), and found that HONO simulations were significantly improved. However, Li et al. (2010) used a relatively high emissions ratio of 2.3 % for HONO / NO₂ to compute the direct emissions of HONO, which could have overestimated the HONO concentrations in the air (An et al., 2013). Czader et al. (2012) added Reactions (R6), (R7), and HONO emissions into the CMAQ model. The HONO simulations matched well with observations at night, but were significantly lower than observations at noon. Wong et al. (2013) reported good agreement between simulated and observed daytime HONO when HONO emissions, photolytically enhanced daytime formation mechanisms on both aerosols and the ground, and Reaction (R7), were included. However, according to our recent studies (Tang et al., 2014), this result depended heavily on the selection of uptake coefficients of NO₂ heterogeneous chemistry. Overall, the topic of HONO sources remains under discussion today, and so it is a challenge for modelers to decide which mechanism(s) to be coupled into an air quality model.

To investigate the importance of the mechanisms described above, correlation tests between the P_{unknown} and NO₂, HNO₃, irradiation or the photolysis frequency of NO₂ [$J(\text{NO}_2)$], were conducted in field experiments (Acker and Möller, 2007; Sörgel et al., 2011; Villena et al., 2011; Wong et al., 2012). Many of these studies demonstrated that there is a clear dependency of the P_{unknown} on irradiation / $J(\text{NO}_2)$ during daytime, particularly at noon. Rohrer et al. (2005) proposed that the photolytic HONO source at the surface of

the chamber strongly depended on light intensity. Acker and Möller (2007) summarized field experiments in several European countries and showed a strong correlation ($R^2 = 0.81$) between the P_{unknown} and $J(\text{NO}_2)$. Wong et al. (2012) also indicated that the P_{unknown} showed a clear symmetrical diurnal variation with a maximum around noontime, closely correlated with actinic flux (NO₂ photolysis frequency) and solar irradiance; the correlation coefficient was over 0.70.

Besides irradiation / $J(\text{NO}_2)$, good correlations between the P_{unknown} and NO₂ mixing ratios have been found from both field and laboratory studies, supporting the viewpoint that NO₂ is the primary precursor of HONO. Through estimating the P_{unknown} , Acker and Möller (2007) speculated that the daytime HONO levels might be explained by a fast electron transfer onto adsorbed NO₂. Sörgel et al. (2011) indicated that the conversion of NO₂ most likely accounted for light-induced HONO formation, about an order of magnitude stronger than HONO formation during nighttime. High correlations between the P_{unknown} and NO₂ mixing ratios have also been found (e.g., $R^2 = 0.77$ in Qin et al., 2006, $R^2 = 0.80$ in Villena et al., 2011, and $R^2 = 0.62$ in Elshorbany et al., 2009), indicating that the photosensitized conversion of NO₂ is more likely to be the daytime HONO source. This is the reason why the recent CalNex 2010 (California Research at the Nexus of Air Quality and Climate Change) study found a very strong positive correlation ($R^2 = 0.985$) between HONO flux and the product of NO₂ concentration and solar radiation at the Bakersfield site (Ren et al., 2011).

Based on the studies introduced above, the P_{unknown} calculated from field experiments may be a practical method to help quantify the daytime HONO source. In this study, field

experiment data from 13 different field campaigns across the globe were used to express the P_{unknown} as a function of NO₂ mixing ratios and $J(\text{NO}_2)$ (see Sect. 2.2). We then added the P_{unknown} into the WRF-Chem model to assess the impacts of the P_{unknown} on the concentrations and production and loss rates of HONO, OH, HO₂, and organic peroxy radicals (RO₂).

2 Data and methods

2.1 Observed data

Anthropogenic emissions were based on the year 2006/2007. Limited measurements of HONO, OH, and HO₂ in the coastal regions of China were made in the summers of 2006/2007, so these limited measurements were used for model evaluation. Observed air temperature (TA), relative humidity (RH), wind speed (WS), and direction (WD) near the ground were obtained from the National Climatic Data Center, China Meteorological Administration (H. Zhang et al., 2012). Surface mixing ratios of O₃ and NO₂ in Beijing were obtained from the Beijing Atmospheric Environmental Monitoring Action, carried out by the Chinese Academy of Sciences (Li et al., 2011; Wang et al., 2014), except those in Guangzhou, which were sourced from Qin et al. (2009). HONO observations were conducted using two annular denuders at the campus of Peking University (39°59' N, 116°18' E) in Beijing on 17–20 August 2007 (Spataro et al., 2013) and a long path absorption photometer at the Backgarden (BG) supersite (23°30' N, 113°10' E), about 60 km northwest of Guangzhou on 3–31 July 2006 (X. Li et al., 2012). The measurement systems are described in detail in Spataro et al. (2013) and X. Li et al. (2012). OH and HO₂ were measured by laser-induced fluorescence at the BG supersite on 3–30 July 2006 (Lu et al., 2012).

2.2 Parameterization of HONO sources

Besides HONO gas-phase production from Reaction (R1), three additional HONO sources [HONO emissions, Reaction (R4) (nighttime), and the P_{unknown}] were coupled into the WRF-Chem model in this work.

HONO emissions were calculated using $[0.023 \times f_{\text{DV}} + 0.008 \times (1 - f_{\text{DV}})] \times f_{\text{TS}}$, where f_{DV} denotes the nitrogen oxides (NO_x) emissions ratio of diesel vehicles to total vehicles, and f_{TS} is the NO_x emissions ratio of the traffic source to all anthropogenic sources (Li et al., 2011; An et al., 2013; Tang et al., 2014). Reaction (R4) was inserted into the Carbon-Bond Mechanism Z (CBM-Z) during nighttime only. The heterogeneous reaction rate was parameterized by $k = \left(\frac{a}{D_g} + \frac{4}{v\gamma}\right)^{-1} A_s$ (Jacob, 2000), where a is the radius of aerosols, v is the mean molecular speed of NO₂, D_g is a gas-phase molecular diffusion coefficient taken as $10^{-5} \text{ m}^2 \text{ s}^{-1}$ (Dentener and Crutzen, 1993), and A_s is the aerosol surface

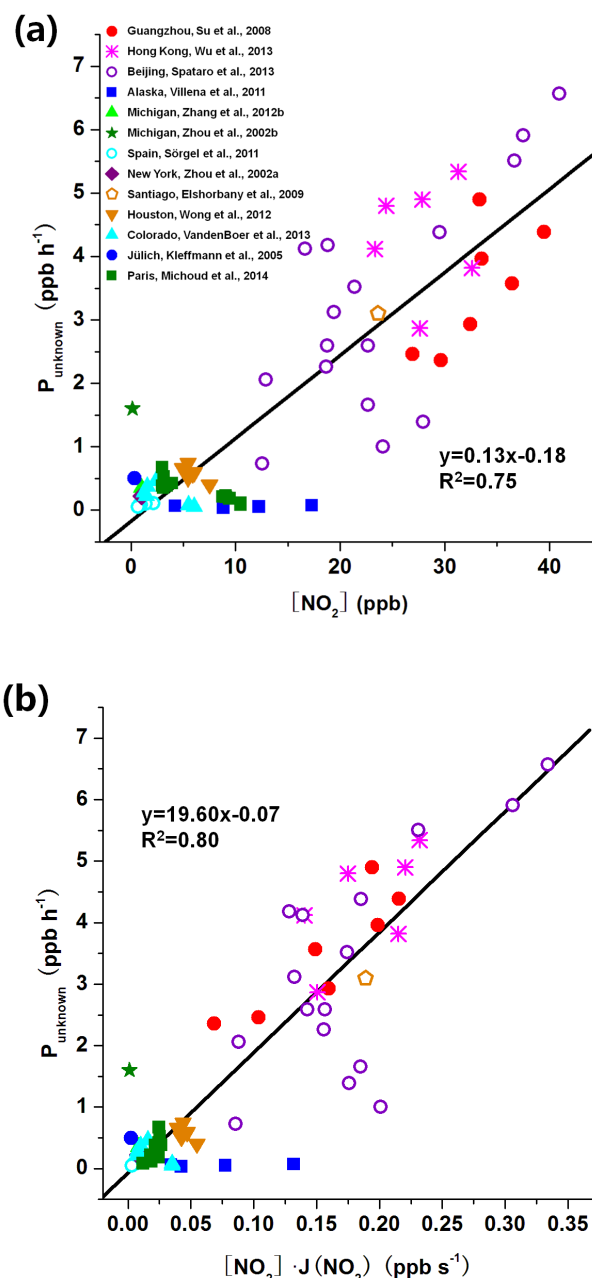


Figure 2. Correlation of the unknown daytime HONO source (P_{unknown}) (ppb h⁻¹) with (a) $[\text{NO}_2]$ (ppb) and (b) $[\text{NO}_2] \times J(\text{NO}_2)$ (ppb s⁻¹), based on the field experiment data shown in Fig. 1.

area per unit volume of air, calculated from aerosol mass concentrations and number density in each bin set by the Model for Simulating Aerosol Interactions and Chemistry (MOSAIC). Hygroscopic growth of aerosols was considered (Li et al., 2011).

Previous studies (Sörgel et al., 2010; Villena et al., 2011; Wong et al., 2012) have shown $P_{\text{unknown}} \propto [\text{NO}_2] \cdot J(\text{NO}_2)$. To quantify the relationship between the P_{unknown} and NO₂

mixing ratios and irradiation, daytime P_{unknown} , NO₂ mixing ratios and $J(\text{NO}_2)$, based on all the available data sets from 13 different field campaigns across the globe (Table S1 in the Supplement), were plotted in Fig. 2. As expected, good correlation ($R^2 = 0.75$) between the P_{unknown} and NO₂ mixing ratios was obtained (Fig. 2a). Furthermore, the correlation (R^2) between the P_{unknown} and $[\text{NO}_2] \cdot J(\text{NO}_2)$ was increased to 0.80, with a linear regression slope of 19.60 (Fig. 2b). For the coastal regions of China (mainly including Liaoning, Beijing, Tianjin, Hebei, Shandong, Jiangsu, Anhui, Shanghai, Zhejiang, Jiangxi, Fujian, and Guangdong), the correlation between the P_{unknown} and $[\text{NO}_2] \cdot J(\text{NO}_2)$ was 0.48, with a linear regression slope of 17.37 (Fig. S2b in the Supplement), which is within the maximum P_{unknown} uncertainty range of 25 % (Table S1). The P_{unknown} could be expressed as a function of NO₂ mixing ratios and $J(\text{NO}_2)$, i.e., $P_{\text{unknown}} \approx 19.60[\text{NO}_2] \cdot J(\text{NO}_2)$. This formula is very similar to $P_{\text{unknown}} \approx \alpha \cdot J(\text{NO}_2) \cdot [\text{NO}_2] \cdot [\text{H}_2\text{O}] \cdot (S/V_g + S/V_a)$ proposed by Su et al. (2008), and $P_{\text{unknown}} \approx 3.3 \times 10^{-8}[\text{NO}_2] \cdot Q_s$ suggested by Wong et al. (2012) as an additional daytime source of HONO through analysis of observed data, where S/V_a is the aerosol surface area-to-volume ratio, S/V_g is the ground surface area-to-volume ratio, α is a fitting parameter, and Q_s is solar visible irradiance. Recently, Li et al. (2014) suggested that high HONO mixing ratios in the residual layer in the studied Po Valley in Italy were mainly from a gas-phase source (S_{HONO}) that consumed NO_x (Li et al., 2015), and S_{HONO} was proportional to the photolysis frequency of HONO [$J(\text{HONO})$], basically consistent with our result that the P_{unknown} was proportional to NO₂ mixing ratios and the photolysis frequency of NO₂ [$J(\text{NO}_2)$].

2.3 Model setup

The WRF-Chem model version 3.2.1 (Grell et al., 2005; Fast et al., 2006), with the CBM-Z (Zaveri and Peters, 1999) and the MOSAIC (Zaveri et al., 2008), was used in this study. The detailed physical and chemical schemes for the simulations can be found in Tang et al. (2014). Two domains with a horizontal resolution of 27 km were employed in this study: domain 1 covered East Asia, whereas domain 2 covered the coastal regions of China, including the Beijing–Tianjin–Hebei region (BTH), the Yangtze River delta (YRD), and the Pearl River delta (PRD) (Fig. 3), which are the three most rapidly developing economic growth regions of China. Rapid economic development and urbanization has led to a serious deterioration in air quality in these three regions. Beijing, Shanghai, and Guangzhou are three representative cities of the three regions, so this study focuses on the three regions, including the three representative cities. There were 28 vertical model layers from the ground to 50 hPa, and the first model layer was ~ 28 m above the ground. Meteorological initial and boundary conditions were obtained from the NCEP (National Centers for Environmental Prediction) $1^\circ \times 1^\circ$ reanalysis data set. Chemical initial and boundary

conditions were constrained with the output of MOZART-4 (Model for Ozone and Related chemical Tracers, version 4) (Emmons et al., 2010), every 6 h. Monthly anthropogenic emissions in 2006/2007 and biogenic emissions were the same as those used by Li et al. (2011) and An et al. (2013).

Six simulations (cases R, R_{wop}, and R_p, performed for the entire months of August 2007 and July 2006), with a spin-up period of 7 days, were conducted to assess the P_{unknown} effects on the concentrations and budgets of HONO, OH, HO₂, and RO₂. Case R only considered Reaction (R1) as a reference; Case R_{wop} included case R with HONO emissions, and Reaction (R4) only at night; case R_p contained case R_{wop} with the $P_{\text{unknown}} [\approx 19.60[\text{NO}_2] \cdot J(\text{NO}_2)]$. The P_{unknown} and Reaction (R4) were added to the CBM-Z, and diagnostic variables (i.e., production and loss rates of HONO, OH, HO₂, RO₂, O₃, and other species) were inserted into the CBM-Z to quantify the P_{unknown} impacts on the budgets of HONO, OH, HO₂, and RO₂ (Wang et al., 2014).

3 Results and discussion

3.1 Comparison of simulations and observations

The statistical metrics of mean bias (MB), mean error (ME), root-mean-square error (RMSE), normalized mean bias (NMB), normalized mean error (NME), index of agreement (IOA), and correlation coefficient (CC), were used. The MB, ME, and RMSE are given in the same units as the measurements (absolute metrics). The MB quantifies the tendency of the model to over- or underestimate values, while the ME and RMSE measure the magnitude of the difference between modeled and observed values, regardless of whether the modeled values are higher or lower than observations. One disadvantage of absolute metrics is that they make intercomparisons of model performance in clean and polluted environments or across different pollutants difficult to interpret. Consequently, a range of relative metrics are often used. These metrics are presented either in fractional or percentage units. The NMB and NME all normalize by observed values. The IOA and CC provide a sense of the strength of the relationship between model estimates and observations that have been paired in time and space. Perfect agreement for any metric alone may not be indicative of good model performance, so multiple metrics must be considered when evaluating model performance. Simulations of TA, RH, WS and WD were compared with observations, as shown in Wang et al. (2014). The MB, ME, RMSE, NMB, NME, IOA, and CC were comparable with those of Wang et al. (2010) and L. Li et al. (2012) using MM5 (the fifth-generation Pennsylvania State University/National Center for Atmospheric Research Mesoscale Model), and H. Zhang et al. (2012) using the WRF model. For O₃ in Beijing of the BTH region and Guangzhou of the PRD region, the NMB, NME, and IOA were -22.80 , 58.70 , and 0.79 %, respectively (Table 1

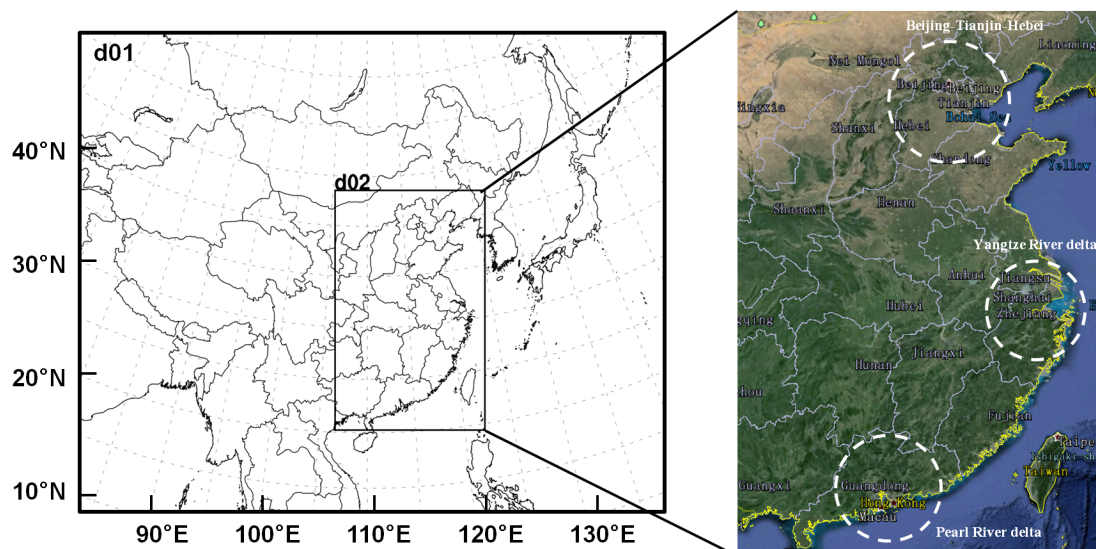


Figure 3. Model domains used in this study. Domain 2 covers the Beijing–Tianjin–Hebei (BTH), Yangtze River delta (YRD), and Pearl River delta (PRD) regions.

Table 1. Model performance statistics for O₃ and NO₂ in Beijing in August 2007 and Guangzhou in July 2006.

Species	Case	MB (ppb)	ME (ppb)	RMSE (ppb)	NMB (%)	NME (%)	IOA
O ₃	R _p	−0.65	19.40	25.44	−2.20	66.10	0.80
	R	−6.69	17.21	25.24	−22.80	58.70	0.79
NO ₂	R _p	−9.50	17.31	21.40	−29.10	53.00	0.51
	R	−4.40	13.75	17.61	−13.50	42.10	0.57

MB: mean bias; ME: mean error; RMSE: root-mean-square error; NMB: normalized mean bias; NME: normalized mean error; IOA: index of agreement.

for case R), comparable to the values of 30.2 % for NMB, 55.8 % for NME, and 0.91 for IOA, reported in L. Li et al. (2012) using the CMAQ model. When HONO emissions, Reaction (R4), and the P_{unknown} were included, the NMB, NME, and IOA increased to −2.20, 66.10 %, and 0.80, respectively (Table 1 for case R_p). The NO₂ fluctuations were generally captured (Fig. 4) but the simulated amplitude of NO₂ was underestimated in some cases (Fig. 4). This underestimation could be related to the uncertainty of NO_x emissions. For NO₂ in case R, the NMB, NME, and IOA were −13.50, 42.10 %, and 0.57, respectively (Table 1), similar to the results of Wang et al. (2010) using the CMAQ model (NMB of −33.0 %, NME of 50.0 %, and IOA of 0.61). Compared with case R, NO₂ simulations (Table 1 for case R_p) were further underestimated for case R_p due to the underestimation of NO_x emissions in Guangzhou.

HONO simulations only with the gas-phase production (case R) were always substantially underestimated compared with observations (Fig. 5), similar to the results of Sarwar et al. (2008), Li et al. (2011), and An et al. (2013). When HONO emissions and Reaction (R4) were included,

HONO simulations were significantly improved, especially at night (Fig. 5 and Table 2 for case R_{wop}). For Beijing, the nighttime RMSE and NME were reduced by 0.90×10^6 molecules cm^{−3} and 44.70 %, whereas the NMB and IOA were increased by 50.00 % and 0.29, respectively (Table 2). For Guangzhou, the nighttime RMSE and NME were reduced by 0.44×10^6 molecules cm^{−3} and 32.90 %, and the NMB and IOA were enhanced by 58.80 % and 0.18, respectively. When the P_{unknown} was included, daytime HONO simulations were considerably improved (Fig. 5 and Table 2 for case R_p). Compared with case R_{wop}, the daytime NME in Beijing was reduced by 19.60 %, and the NMB and IOA in Beijing were increased to −24.30 from −62.00 % and 0.73 from 0.64, respectively (Table 2); the daytime NME in Guangzhou was reduced by 8.10 %, and the NMB in Guangzhou was increased to −61.20 from −76.50 % (Table 2).

Simulated diurnal variations of OH and HO₂ showed consistent patterns with the observed data (Fig. 6). When HONO emissions and Reaction (R4) were considered (case R_{wop}), OH and HO₂ enhancements were $\leq \sim 6$ % in most cases compared with case R (Fig. 6 and Table 3), but the P_{unknown} led to 10–150 % improvements in OH simulations on 5–12 July 2006 (Fig. 6). The 20–90 % overestimation of OH mixing ratios on 20–25 July 2006 (Fig. 6) needs further investigation. Compared with case R, the NME was reduced by 79.60 % (i.e., 136.60 − 57.00 %), whereas the NMB was increased by 105.40 % (123.00 − 17.60 %), and the IOA was improved to 0.84 from 0.79 (Table 3). When the P_{unknown} was considered, HO₂ simulations were substantially improved (Fig. 6), the IOA was improved to 0.61 from 0.54, and the CC was improved to 0.66 from 0.57 (Table 3). However, HO₂ simulations were still substantially underestimated (Fig. 6).

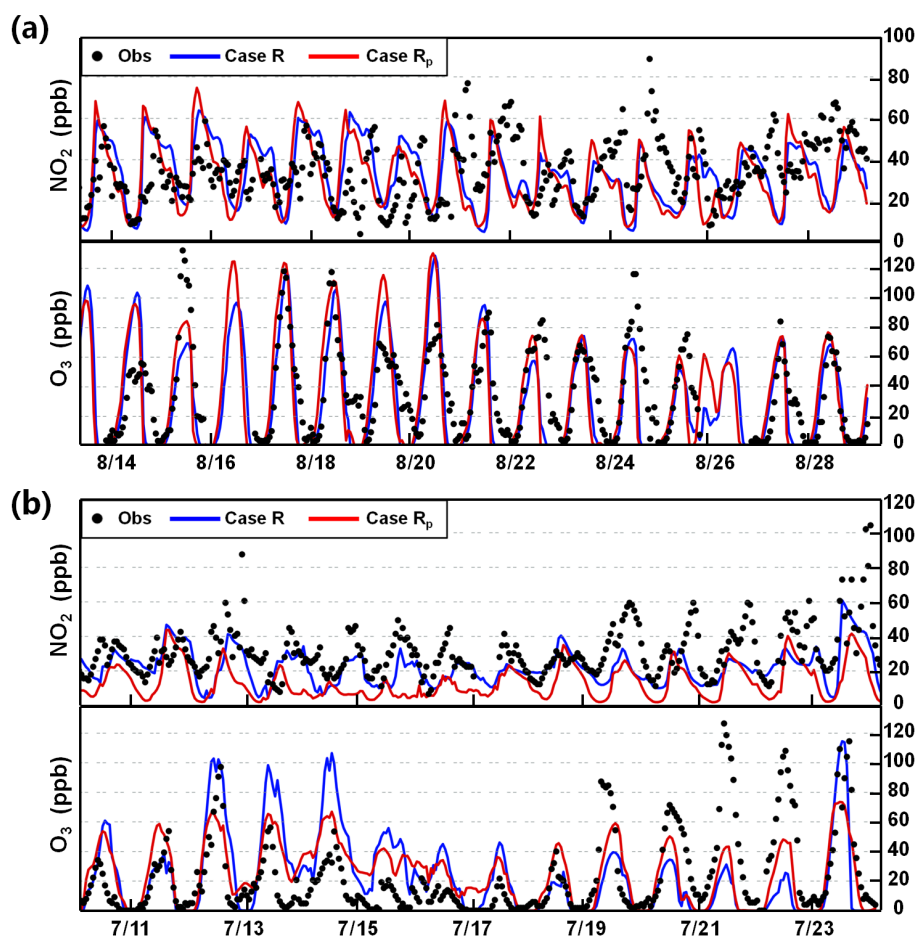


Figure 4. Comparison of simulated and observed hourly mean mixing ratios of NO₂ and O₃ in (a) Beijing on 14–28 August 2007 and (b) Guangzhou on 11–23 July 2006.

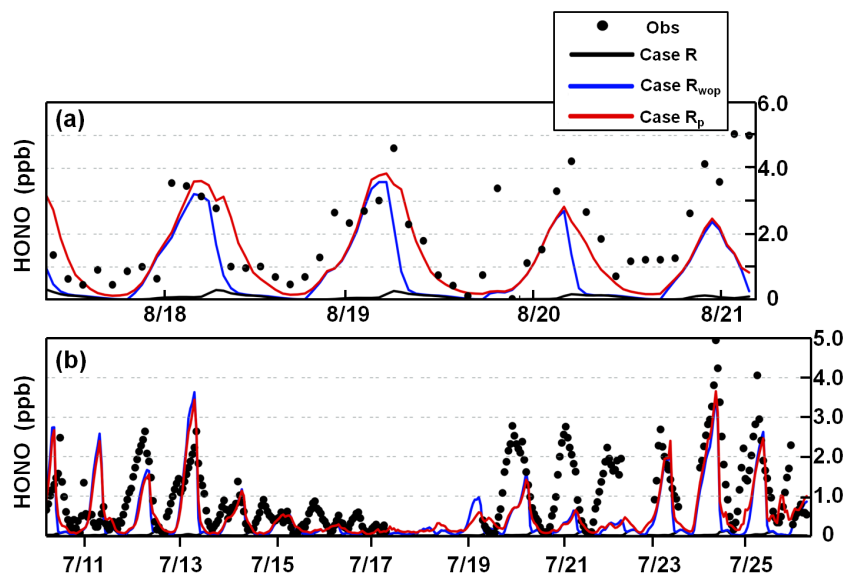
Table 2. Model performance statistics for daytime (06:00–18:00 LST) and nighttime (19:00–05:00 LST) HONO in Beijing in August 2007 and Guangzhou in July 2006.

Species	Case	MB	ME	RMSE	NMB	NME	IOA	CC
		(10 ⁶ molec cm ⁻³)	(10 ⁶ molec cm ⁻³)	(10 ⁶ molec cm ⁻³)	(%)	(%)		
HONO _{daytime} (Beijing)	R _p	−0.54	0.98	1.41	−24.30	44.50	0.73	0.57
	R _{wop}	−1.37	1.41	1.83	−62.00	64.10	0.64	0.63
	R	−2.07	2.07	2.58	−93.80	93.80	0.46	0.31
HONO _{nighttime} (Beijing)	R _p	−0.73	0.84	1.09	−42.20	49.10	0.77	0.74
	R _{wop}	−0.82	0.91	1.16	−47.90	53.20	0.75	0.75
	R	−1.68	1.68	2.06	−97.90	97.90	0.46	0.76
HONO _{daytime} (Guangzhou)	R _p	−0.38	0.43	0.58	−61.20	69.60	0.58	0.56
	R _{wop}	−0.48	0.49	0.65	−76.50	77.70	0.55	0.56
	R	−0.60	0.60	0.80	−95.60	96.20	0.43	−0.30
HONO _{nighttime} (Guangzhou)	R _p	−0.42	0.75	1.05	−32.90	58.50	0.66	0.43
	R _{wop}	−0.49	0.83	1.15	−38.40	64.30	0.63	0.38
	R	−1.25	1.25	1.59	−97.20	97.20	0.45	−0.01

CC: correlation coefficient.

Table 3. Model performance statistics for OH and HO₂ in Guangzhou in July 2006.

Species	Case	MB (10 ⁶ molec cm ⁻³)	ME (10 ⁶ molec cm ⁻³)	RMSE (10 ⁶ molec cm ⁻³)	NMB (%)	NME (%)	IOA	CC
OH	R _p	-1.35	4.37	6.22	-17.60	57.00	0.84	0.75
	R _{wop}	-3.00	4.58	6.25	-112.20	126.50	0.81	0.72
	R	-3.36	4.85	6.55	-123.00	136.60	0.79	0.70
HO ₂	R _p	-3.80	3.81	5.59	-78.50	78.60	0.61	0.66
	R _{wop}	-4.19	4.20	6.14	-86.60	86.70	0.54	0.59
	R	-4.22	4.23	6.16	-87.20	87.30	0.54	0.57

**Figure 5.** Comparison of simulated and observed hourly mean HONO mixing ratios at the Peking University site in (a) Beijing on 17–20 August 2007 (Spataro et al., 2013) and (b) the Backgarden site in Guangzhou on 11–25 July 2006 (X. Li et al., 2012).

One of the major reasons for the HO₂ underestimation could be related to the considerable underestimation of anthropogenic volatile organic compounds (VOCs) (Wang et al., 2014).

3.2 P_{unknown} simulations and its impacts on production and loss rates of HONO

High P_{unknown} values were found in the coastal regions of China (Fig. 7), especially in the BTH, YRD, and PRD regions due to elevated emissions of NO_x (Zhang et al., 2009). The largest daytime average P_{unknown} value reached 2.5 ppb h⁻¹ in Tianjin of the BTH region (Fig. 7a), whereas it was 2.0 ppb h⁻¹ in Shanghai of the YRD region (Fig. 7b). The largest daytime average P_{unknown} value reached 1.2 ppb h⁻¹ in Guangzhou and Shenzhen of the PRD (Fig. 7c), lower than the values of 2.5 ppb h⁻¹ and 2.0 ppb h⁻¹. One major reason is the underestimation of daytime NO₂ mixing ratios in the PRD (Fig. 4b).

For case R, daytime HONO production was primarily from the reaction of OH and nitric oxide (NO) (Reaction R1), with a maximum production rate of 0.69 ppb h⁻¹ in Beijing, 1.20 ppb h⁻¹ in Shanghai, and 0.72 ppb h⁻¹ in Guangzhou near noon due to high OH mixing ratios (Fig. 8a, c, e). The loss rate of HONO was 0.62 ppb h⁻¹ in Beijing, 1.09 ppb h⁻¹ in Shanghai, and 0.65 ppb h⁻¹ in Guangzhou via Reaction (R2), much higher than the 0.01–0.02 ppb h⁻¹ in Beijing, Shanghai, and Guangzhou via Reaction (R3) (Fig. 8b, d, f), indicating that Reaction (R2) accounted for approximately 99 % of the total loss rate of HONO.

When the additional HONO sources (HONO emissions, Reaction (R4), and the P_{unknown}) were coupled into the WRF-Chem model, nighttime HONO was formed mainly via Reaction (R4) (0.30–1.42 ppb h⁻¹ in Beijing, 0.20–0.45 ppb h⁻¹ in Shanghai, and 0.25–0.84 ppb h⁻¹ in Guangzhou) (Fig. 8a, c, e). HONO emissions contributed 0.04–0.62 ppb h⁻¹ to HONO production (Fig. 8a, c, e). Simulated P_{unknown} values ranged from 0.42 to 2.98 ppb h⁻¹ in Beijing, from 0.18 to 2.58 ppb h⁻¹ in Shanghai, and from

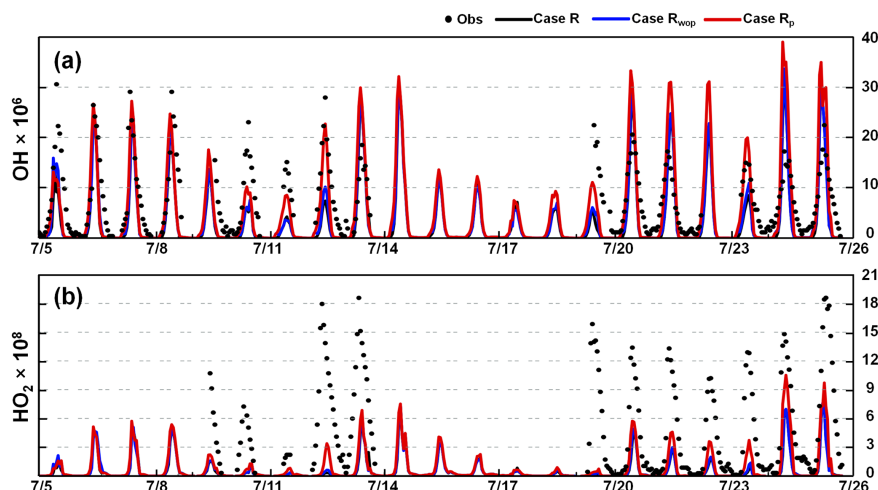


Figure 6. Comparison of simulated and observed hourly mean mixing ratios of OH and HO₂ at the Backgarden site in Guangzhou in July 2006 (Lu et al., 2012).

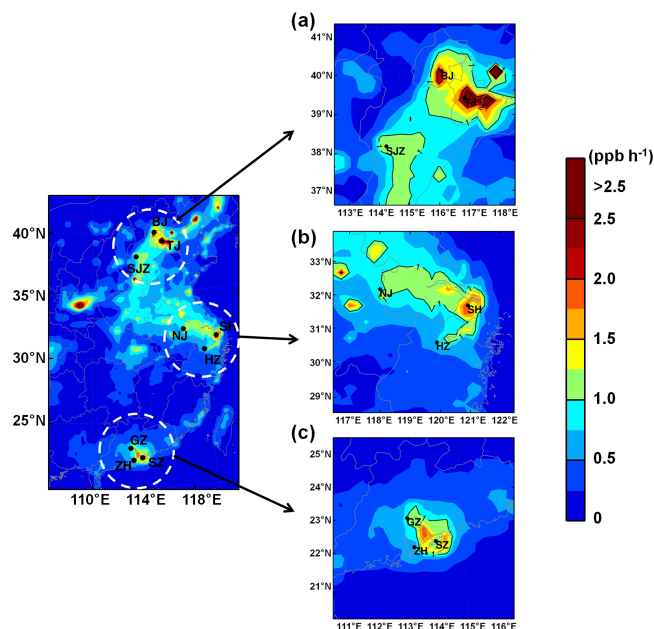


Figure 7. Simulated unknown daytime HONO source (ppb h^{-1}) in the (a) BTH, (b) YRD, and (c) PRD regions in August 2007 (BJ, Beijing; TJ, Tianjin; SJZ, Shijiazhuang; SH, Shanghai; NJ, Nanjing; HZ, Hangzhou; GZ, Guangzhou; ZH, Zhuhai; SZ, Shenzhen).

0.06 to 1.66 ppb h^{-1} in Guangzhou (Fig. 8a, c, e). The simulated P_{unknown} values in Beijing (Fig. 8a) were in good agreement with the results of Spataro et al. (2013), with an average unknown daytime HONO production rate of 2.58 ppb h^{-1} in the studied summer period. However, the simulated P_{unknown} values in Guangzhou (Fig. 8e) were lower than the $2.36\text{--}4.90 \text{ ppb h}^{-1}$ reported by Su et al. (2008), due mainly to the underestimation of the daytime NO₂ mixing ratios in the PRD region. The additional HONO sources produce more

HONO, which subsequently photolyzes to yield more OH. Therefore, the formation of HONO through Reaction (R1) was greatly enhanced, with a maximum of $4.70 [1.44]$ (due to the P_{unknown}) ppb h^{-1} in Beijing, $4.25 [3.13]$ ppb h^{-1} in Shanghai, and $1.58 [0.40]$ ppb h^{-1} in Guangzhou in the morning (Fig. 8a, c, e), much higher than the 0.69 ppb h^{-1} in Beijing, 1.20 ppb h^{-1} in Shanghai, and 0.72 ppb h^{-1} in Guangzhou, respectively, for case R (Fig. 8a, c, e). Meanwhile, the loss rate of HONO via Reaction (R2) was significantly enhanced, with a maximum enhancement of 5.20 (i.e., $5.82 - 0.62$) $[1.97]$ (due to the P_{unknown}) ppb h^{-1} in Beijing, 4.31 (i.e., $5.40 - 1.09$) $[1.44]$ ppb h^{-1} in Shanghai, and 1.96 (i.e., $2.61 - 0.65$) $[1.18]$ ppb h^{-1} in Guangzhou (Fig. 8b, d, f). The HONO loss rate via dry deposition ranged from 0.28 to 0.45 ppb h^{-1} (not shown), roughly equivalent to the contribution of HONO emissions, suggesting that dry deposition of HONO cannot be neglected in high NO_x emission areas. The maximum P_{unknown} uncertainty range of 25% (Table S1), a 25% increase (decrease) in the slope factor (19.60) led to a 9.19–18.62% increase (a 8.40–14.32% decrease) in the maximum production and loss rate of HONO (Fig. S3 in the Supplement).

3.3 P_{unknown} impacts on concentrations of OH, HO₂, and RO₂

Incorporation of the P_{unknown} into the WRF-Chem model led to substantial enhancements in the daytime average mixing ratios of OH in the coastal regions of China, e.g., 60–190% in the BTH region, 60–210% in the YRD region, and 60–200% in the PRD region (Fig. 9a). The maximum enhancement of HO₂ reached 250% in the BTH region, 200% in the YRD region, and 140% in the PRD region (Fig. 9b). Similarly, a daytime average increase of 100–180, 60–150, and 40–80% in RO₂ (i.e., CH₃O₂ (methylperoxy radical) +

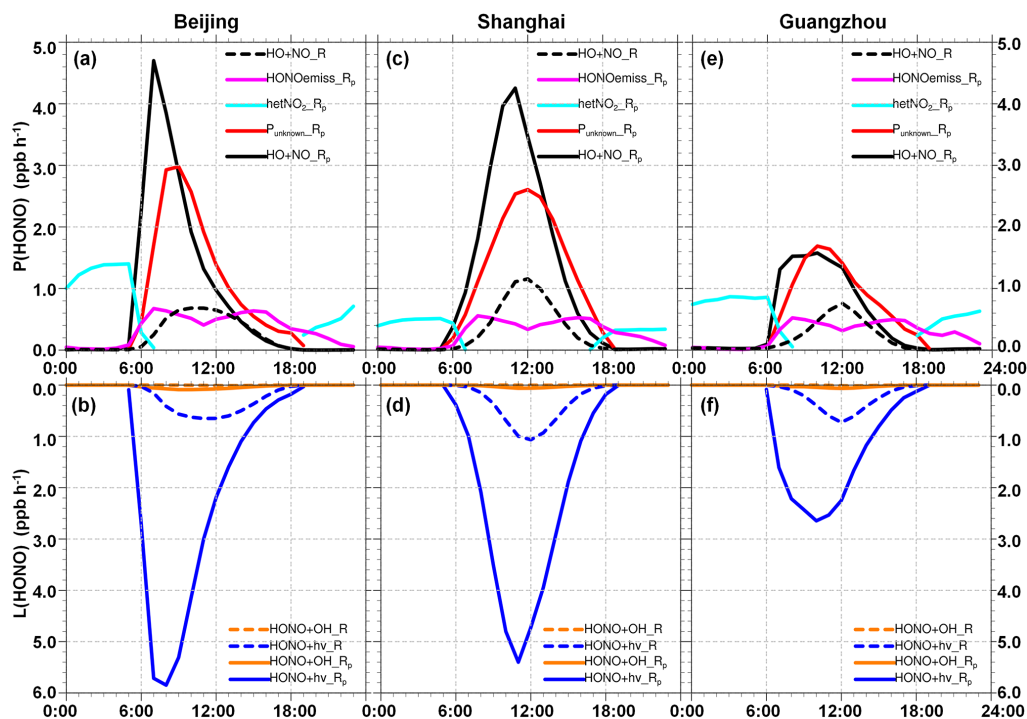


Figure 8. Production [$P(\text{HONO})$] and loss [$L(\text{HONO})$] rates of HONO for cases R (dashed lines) and R_p (solid lines) in (a, b) Beijing, (c, d) Shanghai, and (e, f) Guangzhou in August 2007.

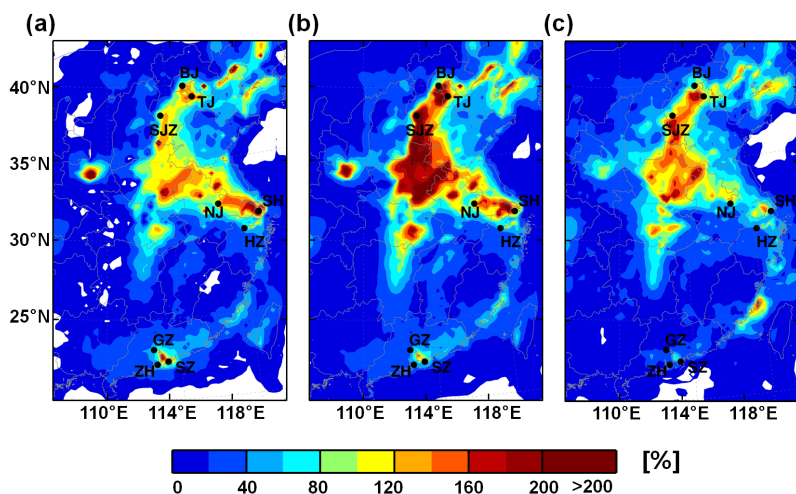


Figure 9. Daytime (06:00–18:00 LST) percentage enhancements of (a) OH, (b) HO₂, and (c) RO₂ due to the unknown daytime HONO source (case R_p – case R_{wop}) in the coastal regions of China in August 2007.

ETHP (ethyl peroxy radical) + C₂O₃ (peroxyacyl radical) + others) were found in the BTH, YRD, and PRD regions, respectively (Fig. 9c).

Vertically, the P_{unknown} enhanced the monthly meridional-mean daytime (06:00–18:00 LST) mixing ratios of OH, HO₂, and RO₂ by 5–38, 5–47, and 5–48 %, respectively, within 1000 m above the ground in the coastal regions of China (Fig. 10). Strong vertical mixing in the daytime in summer

led to a roughly uniform vertical enhancement of OH, HO₂, and RO₂ within 1000 m at the same latitude (Fig. 10). Different P_{unknown} values in different latitudes produced distinct differences in the enhancements of OH, HO₂, and RO₂, with a maximum located near 35° N (Fig. 10).

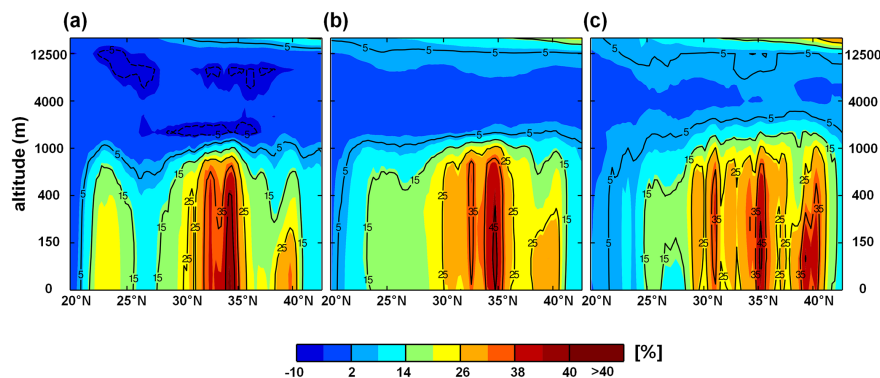


Figure 10. Daytime (06:00–18:00 LST) meridional-mean percentage enhancements of (a) OH, (b) HO₂, and (c) RO₂ due to the unknown daytime HONO source (case R_p – case R_{wop}) in the coastal regions of China in August 2007.

3.4 P_{unknown} impacts on the budgets of OH, HO₂, and RO₂

OH radicals are produced mainly through the reaction of HO₂ + NO, the photolysis of O₃ and HONO, and the reactions between O₃ and alkenes (Fig. 11). For case R, the predominant contribution to P(OH) (production rate of OH) was the reaction of HO₂ + NO (Fig. S1a, c, e), and the photolysis of O₃ was the second most important source of OH (Fig. S1a, c, e). When the three additional HONO sources were added, the most important source was the reaction of HO₂ + NO, with a diurnal maximum conversion rate reaching 9.38 [7.23] (due to the P_{unknown}) ppb h⁻¹ in Beijing, 2.63 [1.15] ppb h⁻¹ in Shanghai, and 4.88 [1.43] ppb h⁻¹ in Guangzhou near noon (Fig. 11a, c, e). The photolysis of HONO became the second most important source of OH in Beijing and Guangzhou before 10:00 LST, and in Shanghai before 12:00 LST; the diurnal peaks were 3.72 [3.06] ppb h⁻¹ in Beijing at 09:00 LST, 0.89 [0.62] ppb h⁻¹ in Shanghai at 11:00 LST, and 0.97 [0.78] ppb h⁻¹ in Guangzhou at 09:00 LST (Fig. 11a, c, e), which were comparable to or lower than the 3.10 ppb h⁻¹ reported by Elshorbany et al. (2009). Kanaya et al. (2009), who also conducted similar studies at Mount Tai (located in a rural area) of China, using an observationally constrained box model, suggested that the reaction of HO₂ + NO was the predominant OH source, with a daytime average of 3.72 ppb h⁻¹, more than the 1.38 ppb h⁻¹ of the photolysis of O₃. Using an observationally constrained box model, Hens et al. (2014) reported similar results in a boreal forest, in which the dominant contributor to OH was the reaction of HO₂ + NO, ranging from 0.23 to 1.02 ppb h⁻¹ during daytime. The production rates of OH in our study were higher than in Kanaya et al. (2009) and Hens et al. (2014) due to higher NO_x emissions in urban areas than in rural areas.

Recently, Li et al. (2014) proposed an assumed HONO source through the reaction between NO₂ and the hydroperoxyl-water complex (HO₂ · H₂O), and suggested

that the impact of HONO on hydrogen oxide radicals (HO_x) budget could be overestimated because this source mechanism consumed HO_x radicals. However, Ye et al. (2015) argued that the HONO yield for the reaction above is too small (with an upper-limit yield of 0.03) to explain the observation of HONO in the study of Li et al. (2014), and Li et al. (2015) agreed that the reaction of HO₂ · H₂O + NO₂ is not a significant HONO source, suggesting that HONO remains an important net OH precursor, as demonstrated by many field studies (e.g., Kleffmann et al., 2005; Acker et al., 2006) and our simulations.

The dominant loss rate of OH was the reaction of OH + NO₂ for both cases R and R_p (Figs. 11b, d, f and S1b, d, f). The diurnal maximum loss rates were 1.98 ppb h⁻¹ in Beijing, 1.12 ppb h⁻¹ in Shanghai, and 1.70 ppb h⁻¹ in Guangzhou for case R (Fig. S1b, d, f), whereas these values were 5.61 [4.38] (due to the P_{unknown}) ppb h⁻¹ in Beijing, 2.00 [1.00] ppb h⁻¹ in Shanghai, and 2.65 [1.02] ppb h⁻¹ in Guangzhou for case R_p (Fig. 11b, d, f). The reactions of OH + VOCs to form HO₂ and RO₂ were the second most important loss path of OH, with a diurnal maximum of 0.75–1.73 ppb h⁻¹ for case R (Fig. S1b, d, f) and 1.57 [0.82] (due to the P_{unknown}) to 5.37 [4.05] ppb h⁻¹ for case R_p in Beijing, Shanghai, and Guangzhou (Fig. 11b, d, f). The third most important OH loss path was the reaction of OH + CO to form HO₂; the diurnal maximum rates were 0.46–1.47 ppb h⁻¹ for case R (Fig. S1b, d, f) and 0.93 [0.49] (due to the P_{unknown}) to 3.58 [2.86] ppb h⁻¹ for case R_p in Beijing, Shanghai and Guangzhou (Fig. 11b, d, f).

The averaged radical conversion rates in the daytime (06:00–18:00 LST) are illustrated in Fig. 12. OH radicals are produced mainly via the photolysis of O₃, HONO, and hydrogen peroxide (H₂O₂), and the reactions between O₃ and alkenes, after which OH radicals enter the RO_x (i.e., OH + HO₂ + RO₂) cycle (Fig. 12 and Tables 4, S2, and S3).

For case R, the reaction of HO₂ + NO was the major source of OH (2.78 ppb h⁻¹ (81.73 % of the total daytime average production rate of OH) in Beijing, 0.73 ppb h⁻¹

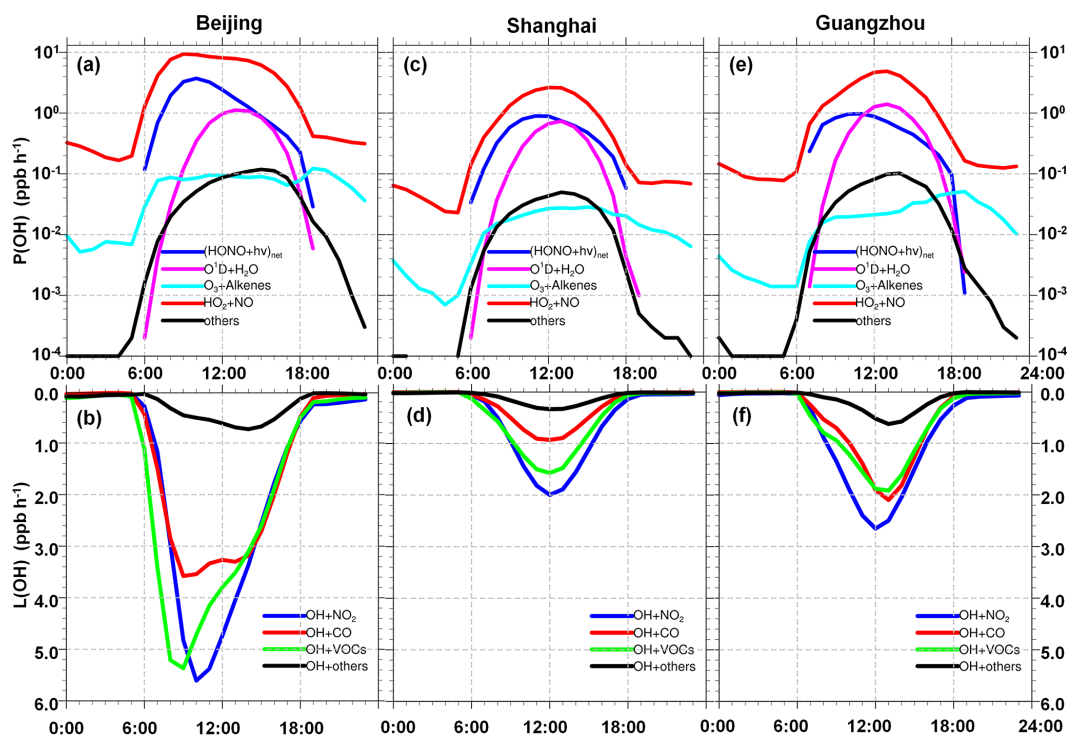


Figure 11. Averaged production [$P(\text{OH})$] and loss [$L(\text{OH})$] rates of OH for case R_p in (a, b) Beijing, (c, d) Shanghai, and (e, f) Guangzhou in August 2007. $(\text{HONO}+h\nu)_{\text{net}}$ means the net OH production rate from HONO photolysis (subtracting OH + NO results in HONO).

(67.09 %) in Shanghai, and 1.75 ppb h^{-1} (71.54 %) in Guangzhou (Fig. 12a and Table 4). The second largest source of OH was the photolysis of O_3 (Table 4). OH radicals were removed mainly through the reaction of OH + NO_2 (1.12 ppb h^{-1} (39.31 % of the total daytime average loss rate of OH) in Beijing, 0.47 ppb h^{-1} (46.63 %) in Shanghai, and 0.77 ppb h^{-1} (38.33 %) in Guangzhou (Table 4), whereas those were converted to HO_2 mainly via the reaction of OH + CO (Table 4). For HO_2 , the predominant production pathways were the reactions of OH + CO and $\text{CH}_3\text{O}_2 + \text{NO}$ and the photolysis of formaldehyde (HCHO) (Table S2). HO_2 radicals were consumed primarily via the reaction of $\text{HO}_2 + \text{NO}$ (2.78 ppb h^{-1} (99.34 %) in Beijing, 0.73 ppb h^{-1} (99.61 %) in Shanghai, and 1.75 ppb h^{-1} (98.29 %) in Guangzhou) (Table S2). RO_2 radicals were formed mainly from the reactions of OH + OLET (terminal olefin carbons)/OLEI (internal olefin carbons), OH + ETH (ethene), OH + methane (CH_4), and OH + AONE (acetone). RO_2 radicals were consumed primarily via the reaction of $\text{CH}_3\text{O}_2 + \text{NO}$ (0.54 ppb h^{-1} (94.56 %) in Beijing, 0.16 ppb h^{-1} (95.28 %) in Shanghai, and 0.33 ppb h^{-1} (96.07 %) in Guangzhou) (Table S3).

When the three additional HONO sources were inserted into the WRF-Chem model (case R_p), the daytime average OH production rate was enhanced by 4.32 (i.e., $7.10 - 2.78$) [3.86] (due to the P_{unknown}) ppb h^{-1} in Beijing, 0.67 (i.e., $1.40 - 0.73$) [0.64] ppb h^{-1} in Shanghai, and 0.80 (i.e.,

$2.55 - 1.75$) [0.68] ppb h^{-1} in Guangzhou via the reaction of $\text{HO}_2 + \text{NO}$, and by 1.86 [1.86] ppb h^{-1} in Beijing, 0.50 [0.50] ppb h^{-1} in Shanghai, and 0.49 [0.47] ppb h^{-1} in Guangzhou via the photolysis of HONO, respectively (Table 4). The enhancements of the daytime average OH production rate due to the photolysis of HONO were comparable to or lower than the 2.20 ppb h^{-1} obtained by Liu et al. (2012). The daytime average OH loss rate was increased by 2.03 [1.92] (due to the P_{unknown}) ppb h^{-1} in Beijing, 0.58 [0.55] ppb h^{-1} in Shanghai, and 0.65 [0.58] ppb h^{-1} in Guangzhou via the reaction of OH + NO_2 , and by 1.78 [1.64] ppb h^{-1} in Beijing, 0.31 [0.28] ppb h^{-1} in Shanghai, and 0.42 [0.36] ppb h^{-1} in Guangzhou via the reaction of OH + CO, respectively (Table 4). Similarly, the daytime average HO_2 production rate was increased by 0.31 [0.28] (due to the P_{unknown}) to 1.78 [1.64] ppb h^{-1} in Beijing, Shanghai and Guangzhou via the reaction of OH + CO, and by 0.63 [0.59] ppb h^{-1} in Beijing, 0.10 [0.09] ppb h^{-1} in Shanghai, and 0.19 [0.17] ppb h^{-1} in Guangzhou via the reaction of $\text{CH}_3\text{O}_2 + \text{NO}$; whereas, the daytime average HO_2 loss rate was enhanced by 0.67 [0.61] (due to the P_{unknown}) to 4.32 [4.27] ppb h^{-1} in Beijing, Shanghai and Guangzhou via the reaction of $\text{HO}_2 + \text{NO}$ (Table S2).

Overall, the net daytime production rate of RO_x was increased to 3.48 (i.e., $2.56 + 0.71 + 0.21$) [2.06] (due to the P_{unknown}) from 1.20 (i.e., $0.60 + 0.43 + 0.17$) ppb h^{-1} in Beijing, 1.09 (i.e., $0.86 + 0.19 + 0.04$) [0.45] from 0.54

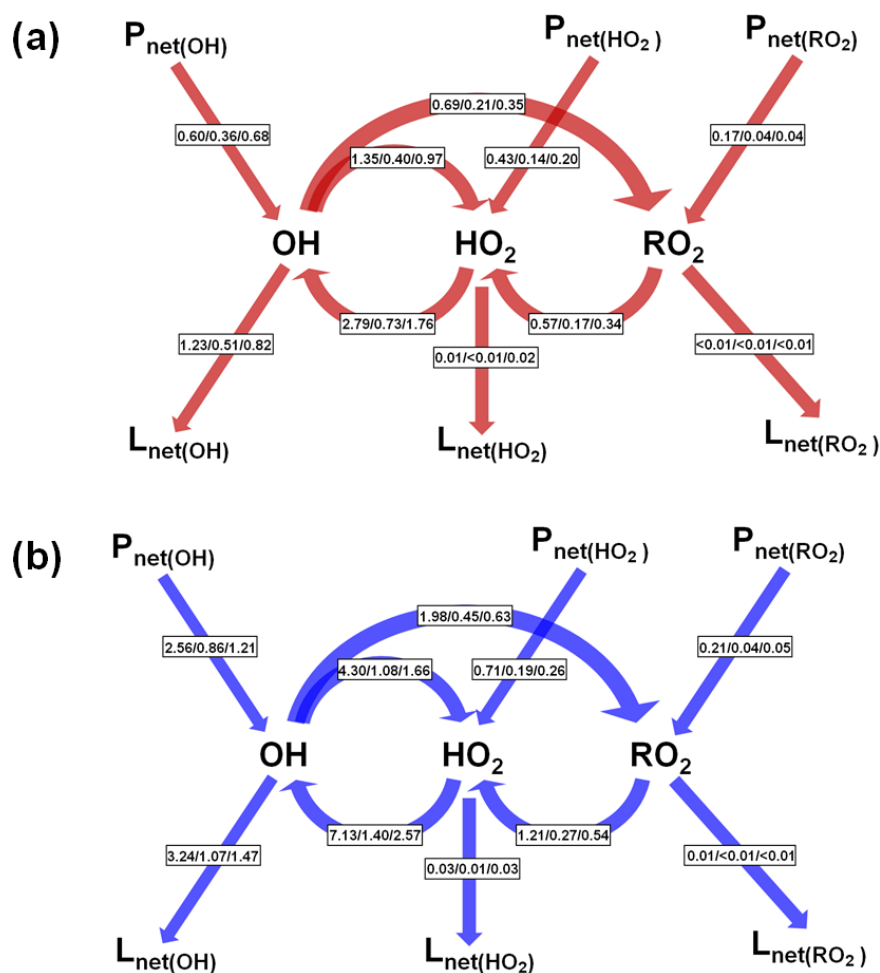


Figure 12. Daytime (06:00–18:00 LST) average budgets of OH, HO₂ and RO₂ radicals (reaction rates, ppb h⁻¹) for cases (a) R and (b) R_p in Beijing/Shanghai/Guangzhou in August 2007.

(i.e., 0.36 + 0.14 + 0.04) ppb h⁻¹ in Shanghai, and 1.52 (i.e., 1.21 + 0.26 + 0.05) [0.58] from 0.92 (i.e., 0.68 + 0.20 + 0.04) ppb h⁻¹ in Guangzhou (Fig. 12) due to the three additional HONO sources, indicating that the RO_x source was mainly from OH production, especially via the photolysis of HONO (Tables 4, S2 and S3). This result is different from the conclusion of Liu et al. (2012) that the photolysis of HONO and oxygenated VOCs is the largest RO_x source. One of the primary reasons for this is the underestimation of anthropogenic VOCs (Wang et al., 2014). For Beijing, the net production rate of RO_x was 3.48 ppb h⁻¹, lower than the 6.60 ppb h⁻¹ from the field studies of Liu et al. (2012). Our results reconfirmed the view of Ma et al. (2012) that the North China Plain acts as an oxidation pool. The additional HONO sources produced an increase of 2.03 [1.96] (due to the P_{unknown}) ppb h⁻¹ in Beijing, 0.56 [0.54] ppb h⁻¹ in Shanghai, and 0.66 [0.59] ppb h⁻¹ in Guangzhou in the net loss rate of RO_x (Fig. 12).

4 Conclusions

The relationship between the P_{unknown} , NO₂ mixing ratios and $J(\text{NO}_2)$ was investigated using available data from 13 field studies across the globe. The formula $P_{\text{unknown}} \approx 19.60[\text{NO}_2] \cdot J(\text{NO}_2)$ was obtained, and then the three additional HONO sources (i.e., the P_{unknown} , HONO emissions and nighttime hydrolysis conversion of NO₂ on aerosols) were inserted into the WRF-Chem model, to assess the P_{unknown} impacts on the concentrations and budgets of HONO and RO_x in the coastal regions of China. The results showed that:

- The additional HONO sources led to significant improvements in the simulations of HONO and OH, especially in the daytime.
- Elevated daytime average P_{unknown} values were found in the coastal regions of China, reaching 2.5 ppb h⁻¹ in the BTH region, 2.0 ppb h⁻¹ in the YRD region, and 1.2 ppb h⁻¹ in the PRD region.

Table 4. Daytime (06:00–18:00 LST) average OH budgets in Beijing/Shanghai/Guangzhou in August 2007. (Major OH production and loss rates and contributions are shown in bold.)

Reaction	Case R		Case R _{wop}		Case R _p	
	Rate (ppb h ⁻¹)	Contribution (%)	Rate (ppb h ⁻¹)	Contribution (%)	Rate (ppb h ⁻¹)	Contribution (%)
OH production						
HO₂+NO	2.778/0.732/1.748	81.73/67.09/71.54	3.242/0.760/1.871	83.74/68.00/72.02	7.101/1.402/2.553	73.34/61.95/67.55
(HONO+ <i>hν</i>) _{net} *	-/-/-	-/-/-	-/-/0.017	-/-/0.66	1.855/0.497/0.489	19.16/21.98/12.93
O¹D+H₂O	0.465/0.307/0.617	13.68/28.17/25.27	0.479/0.306/0.630	12.36/27.38/24.24	0.568/0.312/0.651	5.86/13.80/17.23
O ₃ +OLET/OLEI	0.101/0.024/0.027	2.98/2.16/1.11	0.095/0.023/0.027	2.45/2.08/1.03	0.080/0.021/0.025	0.83/0.91/0.65
(H ₂ O ₂ + <i>hν</i>) _{net} *	0.035/0.023/0.029	1.02/2.07/1.17	0.035/0.023/0.030	0.91/2.03/1.16	0.037/0.022/0.032	0.38/0.97/0.19
HO ₂ +O ₃	0.009/0.001/0.014	0.28/0.07/0.59	0.010/0.001/0.015	0.26/0.06/0.58	0.026/0.001/0.019	0.27/0.05/0.51
(HNO ₃ + <i>hν</i>) _{net} *	0.005/0.001/0.002	0.15/0.06/0.10	0.005/0.001/0.002	0.13/0.06/0.09	0.007/0.001/0.003	0.07/0.04/0.07
ROOH+ <i>hν</i>	0.003/0.004/0.005	0.09/0.36/0.19	0.003/0.004/0.005	0.09/0.38/0.19	0.007/0.007/0.007	0.07/0.29/0.19
O ₃ +ETH	0.002/< 0.001/< 0.001	0.05/0.02/0.01	0.002/< 0.001/< 0.001	0.04/0.02/0.01	0.001/< 0.001/< 0.001	0.02/0.01/0.01
HO ₂ +NO ₃	< 0.001/< 0.001/< 0.001	< 0.01/< 0.01/0.01	< 0.001/< 0.001/< 0.001	< 0.01/< 0.01/< 0.01	< 0.001/< 0.001/< 0.001	< 0.01/< 0.01/< 0.01
O ₃ +ISOP	< 0.001/< 0.001/< 0.001	< 0.01/< 0.01/< 0.01	< 0.001/< 0.001/< 0.001	< 0.01/< 0.01/< 0.01	< 0.001/< 0.001/< 0.001	< 0.01/< 0.01/< 0.01
Total	3.399/1.091/2.443	100/100/100	3.873/1.118/2.598	100/100/100	9.683/2.263/3.779	100/100/100
OH loss						
OH+NO₂	1.116/0.474/0.770	39.31/46.63/38.33	1.225/0.501/0.844	38.11/45.86/38.86	3.146/1.045/1.424	38.08/44.29/40.76
OH+CO	0.785/0.203/0.576	27.65/19.97/28.67	0.932/0.227/0.637	29.00/20.78/29.33	2.573/0.506/1.001	31.14/21.45/28.65
OH+OLET/OLEI	0.192/0.054/0.059	6.76/5.31/2.94	0.264/0.065/0.077	8.21/5.95/3.55	0.537/0.206/0.095	6.50/8.73/2.72
OH+HCHO	0.150/0.050/0.146	5.28/4.92/7.27	0.166/0.053/0.156	5.16/4.85/7.18	0.544/0.096/0.242	6.59/4.07/6.93
OH+CH ₄	0.103/0.057/0.135	3.63/5.61/6.72	0.109/0.059/0.142	3.39/5.40/6.54	0.260/0.115/0.223	3.15/4.87/6.38
OH+ALD2/MGLY/ANOE	0.092/0.018/0.045	3.24/1.77/2.24	0.109/0.020/0.049	3.39/1.83/2.26	0.323/0.047/0.081	3.91/1.99/2.32
OH+SO ₂	0.054/0.030/0.035	1.90/2.95/1.74	0.064/0.034/0.041	1.99/3.11/1.89	0.172/0.116/0.072	2.08/4.92/2.06
OH+XYL	0.052/0.022/0.023	1.83/2.16/1.14	0.066/0.026/0.029	2.05/2.38/1.34	0.141/0.078/0.045	1.71/3.31/1.29
OH+H ₂	0.038/0.021/0.050	1.34/2.07/2.49	0.040/0.022/0.052	1.24/2.01/2.39	0.095/0.027/0.075	1.15/1.14/2.15
OH+TOL	0.027/0.007/0.011	0.95/0.69/0.55	0.034/0.008/0.014	1.06/0.73/0.64	0.086/0.025/0.024	1.04/1.06/0.69
OH+HONO	0.003/0.003/0.005	0.11/0.30/0.25	0.006/0.004/0.007	0.19/0.37/0.32	0.069/0.023/0.032	0.84/0.97/0.92
OH+HNO _x	0.005/0.001/0.005	0.18/0.10/0.25	0.005/0.001/0.005	0.16/0.09/0.23	0.015/0.002/0.008	0.18/0.08/0.23
OH+O ₃	0.028/0.006/0.035	0.99/0.59/1.70	0.029/0.006/0.036	0.90/0.55/1.66	0.072/0.005/0.046	0.87/0.21/1.32
OH+H ₂ O ₂	0.015/0.008/0.027	0.53/0.79/1.34	0.016/0.008/0.029	0.50/0.73/1.34	0.040/0.010/0.043	0.48/0.42/1.23
OH+ETH/OPEN	0.007/0.002/0.004	0.25/0.20/0.20	0.008/0.002/0.005	0.25/0.18/0.23	0.036/0.009/0.011	0.44/0.38/0.31
OH+CH ₃ OOH/ROOH	0.010/0.011/0.014	0.35/1.08/0.70	0.011/0.012/0.014	0.34/1.10/0.64	0.022/0.020/0.022	0.27/0.85/0.63
OH+ISOP	0.019/0.004/0.002	0.67/0.39/0.10	0.020/0.004/0.003	0.62/0.37/0.14	0.017/0.007/0.003	0.21/0.30/0.09
OH+PAR	0.005/0.002/0.004	0.18/0.20/0.20	0.007/0.003/0.005	0.22/0.27/0.23	0.015/0.005/0.007	0.18/0.21/0.20
OH+ONIT/ISOPRD	0.028/0.005/0.016	0.99/0.49/0.80	0.030/0.005/0.018	0.93/0.46/0.83	0.077/0.013/0.025	0.93/0.55/0.72
OH+C ₂ H ₆	0.002/0.001/0.002	0.07/0.10/0.10	0.003/0.001/0.002	0.09/0.09/0.09	0.008/0.002/0.004	0.10/0.08/0.11
OH+CH ₃ OH/AN OL/CRES	0.002/0.001/0.002	0.07/0.10/0.10	0.002/0.001/0.002	0.06/0.09/0.09	0.007/0.002/0.003	0.08/0.08/0.09
OH+HO ₂	0.001/< 0.001/0.004	0.04/0.05/0.20	0.002/< 0.001/0.005	0.06/0.05/0.23	0.006/< 0.001/0.008	0.07/0.02/0.23
OH+NO	0.105/0.036/0.039	3.70/3.54/1.94	0.066/0.030/-	2.05/2.75/-	-/-/-	-/-/-
Total	2.839/1.017/2.009	100/100/100	3.214/1.093/2.172	100/100/100	8.261/2.360/3.495	100/100/100

OLET: terminal olefin carbons (C=C); OLEI: internal olefin carbons (C=C); ROOH: higher organic peroxide; ETH: ethene; ISOP: isoprene; ALD2: acetaldehyde; MGLY: methylglyoxal; ANOE: acetone; XYL: xylene; TOL: toluene; HNO_x: HNO₃+HNO₂; OPEN: aromatic fragments; PAR: paraffin carbon - C-; ONIT: organic nitrate; ISOPRD: lumped intermediate species; ANOL: ethanol; and CRES: cresol and higher molar weight phenols.

* The reactions of HONO+*hν*, H₂O₂+*hν*, and HNO₃+*hν* are reversible. "net" in the subscript denotes the subtraction of the corresponding reverse reactions.

- The additional HONO sources substantially enhanced the production and loss rates of HONO. Dry deposition of HONO contributed 0.28–0.45 ppb h⁻¹ to the loss rate of HONO, approximately equivalent to the contribution of HONO emissions, emphasizing the importance of dry deposition of HONO in high NO_x emissions areas.
- The *P*_{unknown} produced a 60–210% enhancement of OH, a 60–250% enhancement of HO₂, and a 60–180% enhancement of RO₂ near the ground in the major cities of the coastal regions of China. Vertically, the *P*_{unknown} enhanced the daytime meridional-mean mixing ratios of OH, HO₂ and RO₂ by 5–38, 5–47 and 5–48%, respectively, within 1000 m above the ground.
- When the three additional HONO sources were added, the photolysis of HONO became the second most important source of OH in Beijing and Guangzhou before 10:00 LST, and in Shanghai before 12:00 LST, with a maximum of 3.72 [3.06] (due to the *P*_{unknown}) ppb h⁻¹

in Beijing, 0.89 [0.62] ppb h⁻¹ in Shanghai, and 0.97 [0.78] ppb h⁻¹ in Guangzhou; whereas the reaction of HO₂+NO was the most important source of OH which dominated in Beijing and Guangzhou after 10:00 LST and in Shanghai after 12:00 LST, with a maximum of 9.38 [7.23] ppb h⁻¹ in Beijing, 2.63 [1.15] ppb h⁻¹ in Shanghai, and 4.88 [1.43] ppb h⁻¹ in Guangzhou.

Overall, the above results suggest that the *P*_{unknown} significantly enhances the atmospheric oxidation capacity in the coastal regions of China by increasing RO_x concentrations and accelerating RO_x cycles, and could lead to considerable increases in concentrations of inorganic aerosols and secondary organic aerosols and further aggravate haze events in these regions.

The Supplement related to this article is available online at doi:10.5194/acp-15-9381-2015-supplement.

Acknowledgements. This research was partially supported by the National Natural Science Foundation of China (41175105, 41405121), a Key Project of the Chinese Academy of Sciences (XDB05030301), and the Carbon and Nitrogen Cycle Project of the Institute of Atmospheric Physics, Chinese Academy of Sciences, and the Beijing Municipal Natural Science Foundation (8144054).

Edited by: M. Ammann

References

- Acker, K. and Möller, D.: Atmospheric variation of nitrous acid at different sites in Europe, *Environ. Chem.*, 4, 242–255, 2007.
- Acker, K., Möller, D., Wieprecht, W., Meixner, F. X., Bohn, B., Gilge, S., Plass-Dülmer, C., and Berresheim, H.: Strong daytime production of OH from HNO₂ at a rural mountain site, *Geophys. Res. Lett.*, 33, L02809, doi:10.1029/2005GL024643, 2006.
- Alicke, B., Platt, U., and Stutz, J.: Impact of nitrous acid photolysis on the total hydroxyl radical budget during the limitation of oxidant production/Pianura padana produzione di ozono study in Milan, *J. Geophys. Res.-Atmos.*, 107, LOP9-1–LOP9-17, doi:10.1029/2000JD000075, 2002.
- Amedro, D., Parker, A. E., Schoemaeker, C., and Fittschen, C.: Direct observation of OH radicals after 565nm multi-photon excitation of NO₂ in the presence of H₂O, *Chem. Phys. Lett.*, 513, 12–16, 2011.
- Ammann, M., Kalberer, M., Jost, D. T., Tobler, L., Rössler, E., Piguet, D., Gäggeler, H., and Baltensperger, U.: Heterogeneous production of nitrous acid on soot in polluted air masses, *Nature*, 395, 157–160, 1998.
- An, J., Li, Y., Wang, F., and Xie, P.: Impacts of photoexcited NO₂ chemistry and heterogeneous reactions on concentrations of O₃ and NO_y in Beijing, Tianjin and Hebei province of China, *Air Quality-Models and Applications*, edited by: Prof. Dragana Popovic, InTech, ISBN: 978-953-307-307-1, doi:10.5772/16858, 2011.
- An, J., Li, Y., Chen, Y., Li, J., Qu, Y., and Tang, Y.: Enhancements of major aerosol components due to additional HONO sources in the North China Plain and implications for visibility and haze, *Adv. Atmos. Sci.*, 30, 57–66, 2013.
- Atkinson, R. and Aschmann, S. M.: Hydroxyl radical production from the gas-phase reactions of ozone with a series of alkenes under atmospheric conditions, *Environ. Sci. Technol.*, 27, 1357–1363, 1993.
- Carr, S., Heard, D., and Blitz, M.: Comment on “Atmospheric Hydroxyl Radical Production from Electronically Excited NO₂ and H₂O”, *Science*, 324, 5925, doi:10.1126/science.1166669, 2009.
- Crutzen, P. J. and Zimmermann, P. H.: The changing photochemistry of the troposphere, *Tellus B*, 43, 136–151, 1991.
- Czader, B. H., Rappenglück, B., Percell, P., Byun, D. W., Ngan, F., and Kim, S.: Modeling nitrous acid and its impact on ozone and hydroxyl radical during the Texas Air Quality Study 2006, *Atmos. Chem. Phys.*, 12, 6939–6951, doi:10.5194/acp-12-6939-2012, 2012.
- Dentener, F. J. and Crutzen, P. J.: Reaction of N₂O₅ on tropospheric aerosols: Impact on the global distributions of NO_x, O₃, and OH, *J. Geophys. Res.-Atmos.*, 98, 7149–7163, 1993.
- Elshorbany, Y. F., Kurtenbach, R., Wiesen, P., Lissi, E., Rubio, M., Villena, G., Gramsch, E., Rickard, A. R., Pilling, M. J., and Kleffmann, J.: Oxidation capacity of the city air of Santiago, Chile, *Atmos. Chem. Phys.*, 9, 2257–2273, doi:10.5194/acp-9-2257-2009, 2009.
- Emmons, L. K., Walters, S., Hess, P. G., Lamarque, J.-F., Pfister, G. G., Fillmore, D., Granier, C., Guenther, A., Kinnison, D., Laepple, T., Orlando, J., Tie, X., Tyndall, G., Wiedinmyer, C., Baughcum, S. L., and Kloster, S.: Description and evaluation of the Model for Ozone and Related chemical Tracers, version 4 (MOZART-4), *Geosci. Model Dev.*, 3, 43–67, doi:10.5194/gmd-3-43-2010, 2010.
- Fast, J. D., Gustafson, W. I., Easter, R. C., Zaveri, R. A., Barnard, J. C., Chapman, E. G., Grell, G. A., and Peckham, S. E.: Evolution of ozone, particulates, and aerosol direct radiative forcing in the vicinity of Houston using a fully coupled meteorology chemistry aerosol model, *J. Geophys. Res.-Atmos.*, 111, D21305, doi:10.1029/2005JD006721, 2006.
- Finlayson-Pitts, B. J., Wingen, L. M., Sumner, A. L., Syomin, D., and Ramazan, K. A.: The heterogeneous hydrolysis of NO₂ in laboratory systems and in outdoor and indoor atmospheres: An integrated mechanism, *Phys. Chem. Chem. Phys.*, 5, 223–242, 2003.
- Fried, A., McKeen, S., Sewell, S., Harder, J., Henry, B., Goldan, P., Kuster, W., William, E., Baumann, K., Shett, R., and Cantrell, C.: Photochemistry of formaldehyde during the 1993 Tropospheric OH Photochemistry Experiment, *J. Geophys. Res.-Atmos.*, 102, 6283–6296, 1997.
- George, C., Strekowski, R. S., Kleffmann, J., Stemmler, K., and Ammann, M.: Photoenhanced uptake of gaseous NO₂ on solid organic compounds: a photochemical source of HONO?, *Faraday Discuss.*, 130, 195–210, 2005.
- Gonçalves, M., Dabdub, D., Chang, W. L., Jorba, O., and Baldasano, J. M.: Impact of HONO sources on the performance of mesoscale air quality models, *Atmos. Environ.*, 54, 168–176, 2012.
- Grell, G. A., Peckham, S. E., Schmitz, R., McKeen, S. A., Frost, G., Skamarock, W. C., and Eder, B.: Fully coupled “online” chemistry within the WRF model, *Atmos. Environ.*, 39, 6957–6975, 2005.
- Hens, K., Novelli, A., Martinez, M., Auld, J., Axinte, R., Bohn, B., Fischer, H., Keronen, P., Kubistin, D., Nölscher, A. C., Oswald, R., Paasonen, P., Petäjä, T., Regelin, E., Sander, R., Sinha, V., Sipilä, M., Taraborrelli, D., Tatum Ernest, C., Williams, J., Lelieveld, J., and Harder, H.: Observation and modelling of HO_x radicals in a boreal forest, *Atmos. Chem. Phys.*, 14, 8723–8747, doi:10.5194/acp-14-8723-2014, 2014.
- Jacob, D. J.: Heterogeneous chemistry and tropospheric ozone, *Atmos. Environ.*, 34, 2131–2159, 2000.
- Kanaya, Y., Pochanart, P., Liu, Y., Li, J., Tanimoto, H., Kato, S., Suthawaree, J., Inomata, S., Taketani, F., Okuzawa, K., Kawamura, K., Akimoto, H., and Wang, Z. F.: Rates and regimes of photochemical ozone production over Central East China in June 2006: a box model analysis using comprehensive measurements of ozone precursors, *Atmos. Chem. Phys.*, 9, 7711–7723, doi:10.5194/acp-9-7711-2009, 2009.
- Kerbrat, M., Legrand, M., Preunkert, S., Gallée, H., and Kleismann, J.: Nitrous acid at Concordia (inland site) and Dumont d’Urville

- (coastal site), East Antarctica, *J. Geophys. Res.-Atmos.*, 117, D08303, doi:10.1029/2011JD017149, 2012.
- Kleffmann, J., Gavriloaiei, T., Hofzumahaus, A., Holland, F., Koppmann, R., Rupp, L., Schlosser, E., Siese, M., and Wahner, A.: Daytime formation of nitrous acid: A major source of OH radicals in a forest, *Geophys. Res. Lett.*, 32, L05818, doi:10.1029/2005GL022524, 2005.
- Li, G., Lei, W., Zavala, M., Volkamer, R., Dusanter, S., Stevens, P., and Molina, L. T.: Impacts of HONO sources on the photochemistry in Mexico City during the MCMA-2006/MILAGO Campaign, *Atmos. Chem. Phys.*, 10, 6551–6567, doi:10.5194/acp-10-6551-2010, 2010.
- Li, L., Chen, C. H., Huang, C., Huang, H. Y., Zhang, G. F., Wang, Y. J., Wang, H. L., Lou, S. R., Qiao, L. P., Zhou, M., Chen, M. H., Chen, Y. R., Streets, D. G., Fu, J. S., and Jang, C. J.: Process analysis of regional ozone formation over the Yangtze River Delta, China using the Community Multi-scale Air Quality modeling system, *Atmos. Chem. Phys.*, 12, 10971–10987, doi:10.5194/acp-12-10971-2012, 2012.
- Li, S., Matthews, J., and Sinha, A.: Atmospheric hydroxyl radical production from electronically excited NO₂ and H₂O, *Science*, 319, 1657–1660, 2008.
- Li, X., Brauers, T., Häsel, R., Bohn, B., Fuchs, H., Hofzumahaus, A., Holland, F., Lou, S., Lu, K. D., Rohrer, F., Hu, M., Zeng, L. M., Zhang, Y. H., Garland, R. M., Su, H., Nowak, A., Wiedensohler, A., Takegawa, N., Shao, M., and Wahner, A.: Exploring the atmospheric chemistry of nitrous acid (HONO) at a rural site in Southern China, *Atmos. Chem. Phys.*, 12, 1497–1513, doi:10.5194/acp-12-1497-2012, 2012.
- Li, X., Rohrer, F., Hofzumahaus, A., Brauers, T., Häsel, R., Bohn, B., Broch, S., Fuchs, H., Gomm, S., Holland, F., Jäger, J., Kaiser, J., Keutsch, F. N., Lohse, I., Lu, K., Tillmann, R., Wegener, R., Wolfe, G. M., Mentel, T. F., Kiendler-Scharr, A., and Wahner, A.: Missing gas-phase source of HONO inferred from Zeppelin measurements in the troposphere, *Science*, 344, 292–296, 2014.
- Li, X., Rohrer, F., Hofzumahaus, A., Brauers, T., Häsel, R., Bohn, B., Broch, S., Fuchs, H., Gomm, S., Holland, F., Jäger, J., Kaiser, J., Keutsch, F. N., Lohse, I., Lu, K., Tillmann, R., Wegener, R., Wolfe, G. M., Mentel, T. F., Kiendler-Scharr, A., and Wahner, A.: Response to comment on “Missing gas-phase source of HONO inferred from Zeppelin measurements in the troposphere”, *Science*, 348, 1326–1326, 2015.
- Li, Y., An, J., Min, M., Zhang, W., Wang, F., and Xie, P.: Impacts of HONO sources on the air quality in Beijing, Tianjin and Hebei Province of China, *Atmos. Environ.*, 45, 4735–4744, 2011.
- Liu, Z., Wang, Y., Gu, D., Zhao, C., Huey, L. G., Stickel, R., Liao, J., Shao, M., Zhu, T., Zeng, L., Amoroso, A., Costabile, F., Chang, C.-C., and Liu, S.-C.: Summertime photochemistry during CAREBeijing-2007: RO_x budgets and O₃ formation, *Atmos. Chem. Phys.*, 12, 7737–7752, doi:10.5194/acp-12-7737-2012, 2012.
- Lu, K. D., Rohrer, F., Holland, F., Fuchs, H., Bohn, B., Brauers, T., Chang, C. C., Häsel, R., Hu, M., Kita, K., Kondo, Y., Li, X., Lou, S. R., Nehr, S., Shao, M., Zeng, L. M., Wahner, A., Zhang, Y. H., and Hofzumahaus, A.: Observation and modelling of OH and HO₂ concentrations in the Pearl River Delta 2006: a missing OH source in a VOC rich atmosphere, *Atmos. Chem. Phys.*, 12, 1541–1569, doi:10.5194/acp-12-1541-2012, 2012.
- Ma, J. Z., Wang, W., Chen, Y., Liu, H. J., Yan, P., Ding, G. A., Wang, M. L., Sun, J., and Lelieveld, J.: The IPAC-NC field campaign: a pollution and oxidization pool in the lower atmosphere over Huabei, China, *Atmos. Chem. Phys.*, 12, 3883–3908, doi:10.5194/acp-12-3883-2012, 2012.
- Michoud, V., Colomb, A., Borbon, A., Miet, K., Beekmann, M., Camredon, M., Aumont, B., Perrier, S., Zapf, P., Siour, G., Ait-Helal, W., Afif, C., Kukui, A., Furger, M., Dupont, J. C., Haefelin, M., and Doussin, J. F.: Study of the unknown HONO daytime source at a European suburban site during the MEGAPOLI summer and winter field campaigns, *Atmos. Chem. Phys.*, 14, 2805–2822, doi:10.5194/acp-14-2805-2014, 2014.
- Monge, M. E., D’Anna, B., Mazri, L., Giroir-Fendler, A., Ammann, M., Donaldson, D. J., and George, C.: Light changes the atmospheric reactivity of soot, *Pro. Natl. Aca. Sci.*, 107, 6605–6609, 2010.
- Oswald, R., Behrendt, T., Ermel, M., Wu, D., Su, H., Cheng, Y., Breuninger, C., Moravek, A., Mouglin, E., Delon, C., Loubet, B., Pommerening-Röser, A., Sörgel, M., Pöschl, U., Hoffmann, T., Andreae, M. O., Meixner, F. X., and Trebs, I.: HONO emissions from soil bacteria as a major source of atmospheric reactive nitrogen, *Science*, 341, 1233–1235, 2013.
- Paulson, S. E., Sen, A. D., Liu, P., Fenske, J. D., and Fox, M. J.: Evidence for formation of OH radicals from the reaction of O₃ with alkenes in the gas phase, *Geophys. Res. Lett.*, 24, 3193–3196, 1997.
- Platt, U., Perner, D., Harris, G. W., Winer, A. M., and Pitts, J. N.: Observations of nitrous acid in an urban atmosphere by differential optical absorption, *Nature*, 285, 312–314, doi:10.1038/285312a0, 1980.
- Qin, M., Xie, P. H., Liu, W. Q., Li, A., Dou, K., Fang, W., Liu, J., and Zhang, W. J.: Observation of atmospheric nitrous acid with DOAS in Beijing, China, *J. Environ. Sci.*, 18, 69–75, 2006.
- Qin, M., Xie, P., Su, H., Gu, J., Peng, F., Li, S., Zeng, L., Liua, J., Liua, W., and Zhang, Y.: An observational study of the HONO–NO₂ coupling at an urban site in Guangzhou City, South China, *Atmos. Environ.*, 43, 5731–5742, 2009.
- Ren, X., Harder, H., Martinez, M., Leshner, R. L., Oliger, A., Simpas, J. B., Brunea, W. H., Schwab, J. J., Demerjian, K. L., He, Y., Zhou, X., and Gao, H.: OH and HO₂ Chemistry in the urban atmosphere of New York City, *Atmos. Environ.*, 37, 3639–3651, 2003.
- Ren, X., Gao, H., Zhou, X., Crouse, J. D., Wennberg, P. O., Browne, E. C., LaFranchi, B. W., Cohen, R. C., McKay, M., Goldstein, A. H., and Mao, J.: Measurement of atmospheric nitrous acid at Bodgett Forest during BEARPEX2007, *Atmos. Chem. Phys.*, 10, 6283–6294, doi:10.5194/acp-10-6283-2010, 2010.
- Ren, X., Sanders, J. E., Rajendran, A., Weber, R. J., Goldstein, A. H., Pusede, S. E., Browne, E. C., Min, K.-E., and Cohen, R. C.: A relaxed eddy accumulation system for measuring vertical fluxes of nitrous acid, *Atmos. Meas. Tech.*, 4, 2093–2103, doi:10.5194/amt-4-2093-2011, 2011.
- Rohrer, F., Bohn, B., Brauers, T., Brüning, D., Johnen, F.-J., Wahner, A., and Kleffmann, J.: Characterisation of the photolytic HONO-source in the atmosphere simulation chamber SAPHIR, *Atmos. Chem. Phys.*, 5, 2189–2201, doi:10.5194/acp-5-2189-2005, 2005.

- Sarwar, G., Roselle, S. J., Mathur, R., Appel, W., Dennis, R. L., and Vogel, B.: A comparison of CMAQ HONO predictions with observations from the Northeast Oxidant and Particle Study, *Atmos. Environ.*, 42, 5760–5770, 2008.
- Sörgel, M., Regelin, E., Bozem, H., Diesch, J.-M., Drewnick, F., Fischer, H., Harder, H., Held, A., Hosaynali-Beygi, Z., Martinez, M., and Zetzsch, C.: Quantification of the unknown HONO daytime source and its relation to NO₂, *Atmos. Chem. Phys.*, 11, 10433–10447, doi:10.5194/acp-11-10433-2011, 2011.
- Spataro, F., Ianniello, A., Esposito, G., Allegrini, I., Zhu, T., and Hu, M.: Occurrence of atmospheric nitrous acid in the urban area of Beijing (China), *Sci. Total Environ.*, 447, 210–224, 2013.
- Stemmler, K., Ammann, M., Donders, C., Kleffmann, J., and George, C.: Photosensitized reduction of nitrogen dioxide on humic acid as a source of nitrous acid, *Nature*, 440, 195–198, 2006.
- Stemmler, K., Ndour, M., Elshorbany, Y., Kleffmann, J., D’Anna, B., George, C., Bohn, B., and Ammann, M.: Light induced conversion of nitrogen dioxide into nitrous acid on submicron humic acid aerosol, *Atmos. Chem. Phys.*, 7, 4237–4248, doi:10.5194/acp-7-4237-2007, 2007.
- Stone, D., Whalley, L. K., and Heard, D. E.: Tropospheric OH and HO₂ radicals: field measurements and model comparisons, *Chem. Soc. Rev.*, 41, 6348–6404, 2012.
- Su, H., Cheng, Y. F., Shao, M., Gao, D. F., Yu, Z. Y., Zeng, L. M., Slanina, J., Zhang, Y. H., and Wiedensohler, A.: Nitrous acid (HONO) and its daytime sources at a rural site during the 2004 PRIDE-PRD experiment in China, *J. Geophys. Res.-Atmos.*, 113, D14312, doi:10.1029/2007JD009060, 2008.
- Su, H., Cheng, Y., Oswald, R., Behrendt, T., Trebs, I., Meixner, F. X., Andreae, M. O., Cheng, P., Zhang, Y., and Pöschl, U.: Soil nitrite as a source of atmospheric HONO and OH radicals, *Science*, 333, 1616–1618, 2011.
- Tang, Y., An, J., Li, Y., and Wang, F.: Uncertainty in the uptake coefficient for HONO formation on soot and its impacts on concentrations of major chemical components in the Beijing–Tianjin–Hebei region, *Atmos. Environ.*, 84, 163–171, 2014.
- VandenBoer, T. C., Brown, S. S., Murphy, J. G., Keene, W. C., Young, C. J., Pszenny, A. A. P., Kim, S., Warneke, C., de Gouw, J. A., Maben, J. R., Wagner, N. L., Riedel, T. P., Thornton, J. A., Wolfe, D. E., Dubé, W. P., Öztürk, F., Brock, C. A., Grossberg, N., Lefer, B., Lerner, B. Middlebrook, A. M., and Roberts, J. M.: Understanding the role of the ground surface in HONO vertical structure: High resolution vertical profiles during NACHTT-11, *J. Geophys. Res.-Atmos.*, 118, 10155–10171, doi:10.1002/jgrd.50721, 2013.
- Villena, G., Wiesen, P., Cantrell, C. A., Flocke, F., Fried, A., Hall, S. R., Hornbrook, R. S., Knapp, D., Kosciuch, E., Mauldin, R. L., McGrath, J. A., Montzka, D., Richter, D., Ullmann, K., Walega, J., Weibring, P., Weinheimer, A., Staebler, R. M., Liao, J., Huey, L. G., and Kleissmann, J.: Nitrous acid (HONO) during polar spring in Barrow, Alaska: a net source of OH radicals?, *J. Geophys. Res.-Atmos.*, 116, D00R07, doi:10.1029/2011JD016643, 2011.
- Wang, F., An, J., Li, Y., Tang, Y., Lin, J., Qu, Y., Cheng, Y., Zhang, B., and Zhai, J.: Impacts of Uncertainty in AVOC Emissions on the Summer RO_x Budget and Ozone Production Rate in the Three Most Rapidly-Developing Economic Growth Regions of China, *Adv. Atmos. Sci.*, 31, 1331–1342, 2014.
- Wang, X., Zhang, Y., Hu, Y., Zhou, W., Lu, K., Zhong, L., Zeng, L., Shao, M., Hu, M., and Russell, A. G.: Process analysis and sensitivity study of regional ozone formation over the Pearl River Delta, China, during the PRIDE-PRD2004 campaign using the Community Multiscale Air Quality modeling system, *Atmos. Chem. Phys.*, 10, 4423–4437, doi:10.5194/acp-10-4423-2010, 2010.
- Wong, K. W., Oh, H.-J., Lefer, B. L., Rappenglück, B., and Stutz, J.: Vertical profiles of nitrous acid in the nocturnal urban atmosphere of Houston, TX, *Atmos. Chem. Phys.*, 11, 3595–3609, doi:10.5194/acp-11-3595-2011, 2011.
- Wong, K. W., Tsai, C., Lefer, B., Haman, C., Grossberg, N., Brune, W. H., Ren, X., Luke, W., and Stutz, J.: Daytime HONO vertical gradients during SHARP 2009 in Houston, TX, *Atmos. Chem. Phys.*, 12, 635–652, doi:10.5194/acp-12-635-2012, 2012.
- Wong, K. W., Tsai, C., Lefer, B., Grossberg, N., and Stutz, J.: Modeling of daytime HONO vertical gradients during SHARP 2009, *Atmos. Chem. Phys.*, 13, 3587–3601, doi:10.5194/acp-13-3587-2013, 2013.
- Wu, J., Xu, Z., Xue, L., and Wang, T.: Daytime nitrous acid at a polluted suburban site in Hong Kong: Indication of heterogeneous production on aerosol. Proceedings of 12th international conference on atmospheric sciences and applications to air quality, Seoul, Korea, 3–5 June 2013, p. 52, 2013.
- Ye, C., Zhou, X., Pu, D., Stutz, J., Festa, J., Spolaor, M., Cantrell, C., Mauldin, R. L., Weinheimer, A., and Haggerty, J.: Comment on “Missing gas-phase source of HONO inferred from Zeppelin measurements in the troposphere”, *Science*, 348, p. 1326-d, 2015.
- Zaveri, R. A. and Peters, L. K.: A new lumped structure photochemical mechanism for large-scale applications, *J. Geophys. Res.-Atmos.*, 104, 30387–30415, 1999.
- Zaveri, R. A., Easter, R. C., Fast, J. D., and Peters, L. K.: Model for simulating aerosol interactions and chemistry (MOSAIC), *J. Geophys. Res.-Atmos.*, 113, D13204, doi:10.1029/2007JD008782, 2008.
- Zhang, B. and Tao, F.: Direct homogeneous nucleation of NO₂, H₂O, and NH₃ for the production of ammonium nitrate particles and HONO gas, *Chem. Phys. Lett.*, 489, 143–147, 2010.
- Zhang, H., Li, J., Ying, Q., Yu, J. Z., Wu, D., Cheng, Y., Kebin Hed, and Jiang, J.: Source apportionment of PM_{2.5} nitrate and sulfate in China using a source-oriented chemical transport model, *Atmos. Environ.*, 62, 228–242, 2012.
- Zhang, N., Zhou, X., Bertman, S., Tang, D., Alaghmand, M., Shepson, P. B., and Carroll, M. A.: Measurements of ambient HONO concentrations and vertical HONO flux above a northern Michigan forest canopy, *Atmos. Chem. Phys.*, 12, 8285–8296, doi:10.5194/acp-12-8285-2012, 2012.
- Zhang, Q., Streets, D. G., Carmichael, G. R., He, K. B., Huo, H., Kannari, A., Klimont, Z., Park, I. S., Reddy, S., Fu, J. S., Chen, D., Duan, L., Lei, Y., Wang, L. T., and Yao, Z. L.: Asian emissions in 2006 for the NASA INTEX-B mission, *Atmos. Chem. Phys.*, 9, 5131–5153, doi:10.5194/acp-9-5131-2009, 2009.
- Zhou, X., Civerolo, K., Dai, H., Huang, G., Schwab, J., and Demerjian, K.: Summertime nitrous acid chemistry in the atmospheric boundary layer at a rural site in New York State, *J. Geophys. Res.-Atmos.*, 107, ACH13-1–ACH13-11, doi:10.1029/2001JD001539, 2002a.

Zhou, X., He, Y., Huang, G., Thornberry, T. D., Carroll, M. A., and Bertman, S. B.: Photochemical production of nitrous acid on glass sample manifold surface, *Geophys. Res. Lett.*, 29, 261–264, doi:10.1029/2002GL015080, 2002b.

Zhou, X., Gao, H., He, Y., Huang, G., Bertman, S. B., Civerolo, K., and Schwab, J.: Nitric acid photolysis on surfaces in low-NO_x environments: significant atmospheric implications, *Geophys. Res. Lett.*, 30, 2217, doi:10.1029/2003GL018620, 2003.

Zhou, X., Zhang, N., TerAvest, M., Tang, D., Hou, J., Bertman, S., Alaghmand, M., Shepson, P. B., Carroll, M. A., Griffith, S., Dusanter, S., and Stevens, P. S.: Nitric acid photolysis on forest canopy surface as a source for tropospheric nitrous acid. *Nat. Geosci.*, 4, 440–443, 2011.